SUPERCONDUCTING MAGNETS, QUENCH PROTECTION

Superconducting magnets are subject to thermal instability, leading to the loss of superconductivity, known as *quench,* in which the critical values of field, temperature, and current density are exceeded and fail to recover. This phenomenon generally begins in a localized region of the coil, then spreads to the rest of the magnet or magnet system with a "quench propagation velocity." All magnets use some form of composite superconducting wire, in which superconducting filaments carry current in parallel with normal conductor, known as the stabilizer. The stabilizer has the dual purpose of preventing quench in the face of disturbances and of protecting the magnet from excessive temperatures and pressures when unwanted quenches occur. Following a quench, current rapidly transfers from the superconducting material to the stabilizer, since composites are always designed so that the resistance of the stabilizer is much less than that of the superconducting material in its normal state.

In the case of a quench, it is almost never possible to allow continued operation at constant current without unacceptable temperature rises in the magnets. The current must be reduced to zero and the stored energy in the magnet eliminated, either by absorbing the energy within the magnet or by dumping the energy externally. If the energy is dumped externally, it may be absorbed in either warm, generally room temperature, dump circuits, or in cold, generally liquid helium temperature, dump circuits. Some magnets have sufficient enthalpy in their stabilizer and magnetically coupled passive structures to absorb their own stored energy without excessive temperature or pressure rises. In fact, most magnets have sufficient energy, if the ratio of peak local heating to average global heating can be held to acceptably low levels. The peak/average ratio can be controlled by design either by activating internal resistive or inductive heaters or by rapidly dumping or heating all helium coolant in order to guarantee that large portions of the coil will heat up together. The other method of protecting magnets is to dump the magnet energy into an external resistor. This requires an absolutely reliable method of interrupting current flow from the power supply and diverting it into the dump resistor. Both methods require reliable and rapid detection of a quench.

The fundamental limit on protecting magnets against quench is the detection of that quench. This can be particularly difficult in the case of coils in an electromagnetically noisy environment, pulsed coils, and multicoil systems. It is also difficult when the coils are very conservatively stabilized, as is often the case for very large coil systems and buswork. Quench detection systems can be active or passive. Active systems usually involve some sort of balanced voltage bridge. The signal/noise ratios of voltage bridges can be improved by using cowound sensors and active cancellation. Passive systems use transformer-fed heaters to trigger superconducting switches or voltage thresholds to trigger cold diodes.

In order to size a magnet for protection, it is usually necessary to know something about the physics of quench propagation. Different physical theories are needed to predict the spread of quench in potted, pool-boiling, and cable-in-conduit superconductors (CICC). Because of the difficulties in predicting disturbances, initial quench zones, and quench propagation, a conservative design criterion is to assume that local hot spots are adiabatic and that all energy must be dumped externally. For internal quenching, the maximum time to heat a long quench zone with a cowound or surface heater has to be known.

The problem of magnet quench protection is a subset of the generic problem of magnet protection, (1) during normal operation, (2) off-normal conditions such as quench, and (3) faults, whether in the coil, bus, or power supply. The two most fatal flaws are mechanical rupture and electrical arcing. They are often preceded by excessive displacement and/or partial electrical discharges and leakage currents. Flaws that are sometime repairable can end a magnet's useful life when cracks cause leakage of helium under pressure, leakage current causes enough heat to quench the magnet, or displacements create unacceptable field errors. All of the structural design may be considered as part of the magnet protection design. This subject is too vast to be treated here, but should be discussed for specific applications in the articles on Superconducting Magnetic Energy Storage, motors/generators, fusion, and Magnetic Resonance Imaging magnets. The design for electrical integrity will be discussed here, since it isn't discussed elsewhere and because the internal and external voltages during a quench dump are usually significantly higher than those during normal operation.

Finally, we briefly review the actual history of failures to protect magnets. Case histories provide a cautionary tale: this article can only go so far in helping to protect magnets, since most failures are caused by mental lapses that are frequently not design errors.

COIL PROTECTION CIRCUITS

When a superconducting magnet quenches, all of its magnetic energy is converted into heat. If a magnet has enough total mass to absorb the heat and is small enough to guarantee that a quench will propagate into a large fraction of the magnet, then no protection circuits are needed, except to disconnect the power supply, when the current isn't freely circulating. However, when the magnet is too large and stores too much energy to guarantee completely passive protection, some active measure must be taken. The main distinctions between the most commonly used coil protection circuits are whether the dump resistors are internal or external to the cryostat and whether the quench detection is triggered by active logic or passive breakdown of a switch. External dump resistors usually correspond to the design philosophy of saving the magnet by depositing almost all of the energy into a large, inexpensive structure at room temperature. Internal dump resistors are usually designed to lower the peak local to average heating of the magnet to a manageably low level.

External Dump

Neumeyer has recently reviewed the external quench protection circuits for superconducting magnets (1). He schematizes

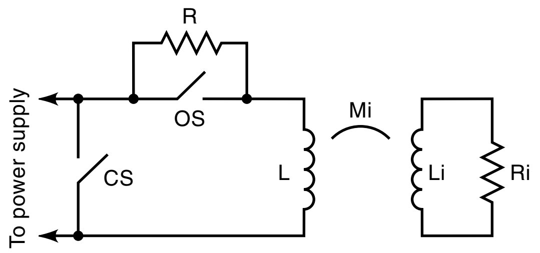

Figure 1. Simple dump circuit schematic [Neumeyer et al. (1)].

the basic external dump circuit as shown in Fig. 1. The magnet is represented by an inductance L, while the mutual inductance M, and the coupled inductance and resistance, L_i and R_i, represent the sum of all coupled magnets and passive conducting structures in the magnet system. The external dump circuit consists of a power supply, a closing switch CS, to shunt out the power supply during quench dump, an opening switch OS to interrupt magnet current, and a dump resistor R (Ω). The basic principle is that the dump resistor is much, much larger than the resistance of the magnet normal zone, so that almost all of the energy is deposited, at room temperature, in a resistor sized to safely absorb all of the magnet energy.

Leads to the dump resistor should generally be coaxial, in order to minimize the voltage overshoot, due to $L_{\text{leads}}\, dI/dt$.

Several equivalent simple dump circuits may be used, as shown in Fig. 2. Under normal operation, they all have the same effect on the magnet. The tradeoffs are in cost versus reliability and in the specifics of the power supply and magnet grounding system. A magnet ground/interrupter switch configuration should be selected that allows the switch and magnet to float on a single short to the magnet case ground without drawing large fault currents.

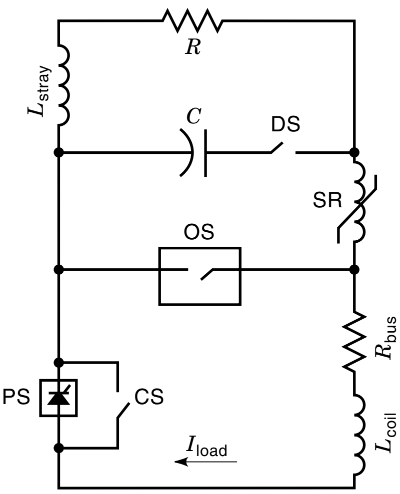

Figure 3. Typical Artificial Zero Counterpulse Circuit [Neumeyer et al. (1)].

Neumeyer represents a typical counterpulse interrupter with the circuit schematic shown in Fig. 3.

The operating coil current flows through the power supply (PS) and the normally closed switch. When a quench is detected, the counterpulse capacitor C is discharged by closing the switch DS, producing a current zero in OS. The inductor SR is a saturable reactor, which desaturates near current zero, decreasing the dI/dt. This helps to extinguish arcs or to restore voltage-holding capability in a solid-state switch. The key parameter, set by selecting the counterpulse capacitor, is the time during which current must be reversed and held near zero. This is on the order of 10 μs for vacuum bottle interrupters, 5 μs to 50 μs for thyristors, and 50 μs to 200 μs for air-blast interrupters. The faster the interrupter clears, the less expensive the counterpulse circuit. For solid-state

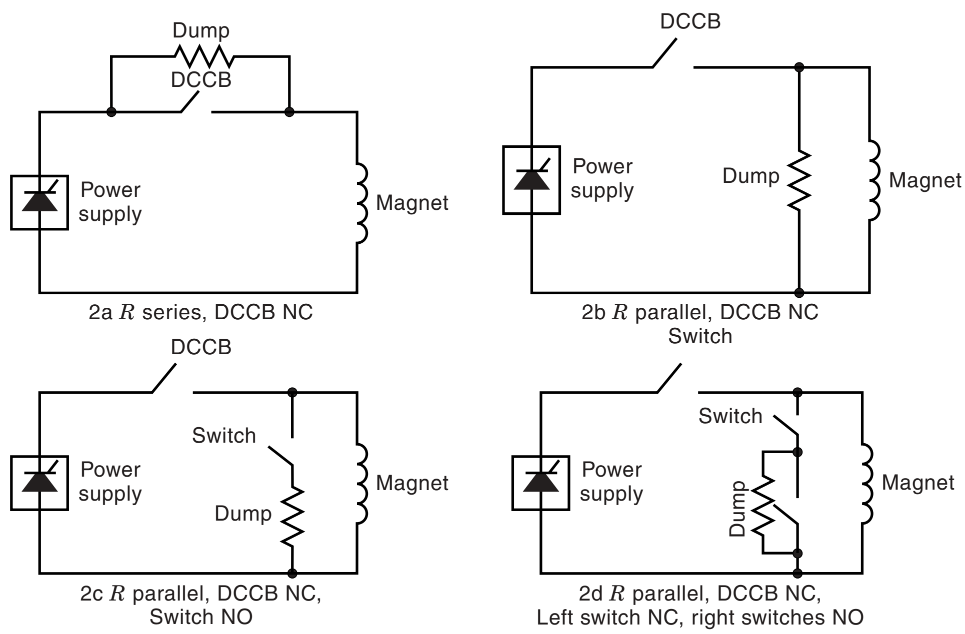

Figure 2. Equivalent superconducting magnet quench dump circuits.

switches with antiparallel diodes, the energy stored in the commutating capacitor must be

$$\frac{1}{2}CV_c^2 = \frac{1}{2}t_{\text{off}}\frac{V(0)I(0)}{\sin\alpha}(\pi - 2\alpha) \tag{1}$$

where t_{off} is the specified time during which reverse voltage is maintained across the solid-state switch (s), α is the phase angle in radians when the switch current is zero, and $V(0) = I(0)\,R$.

The alternative to counterpulsed circuits are dc switches that can sustain a high enough voltage to force current zero without a resonant pulse. Here, the opening switch develops a high enough arc or resistive voltage to drive the device current close enough to zero to extinguish itself and shunt the current to a dump resistor. The most commonly used forced current zero devices are air-blast breakers and explosive switches. The air-blast breakers use a blast of compressed air and rapidly parting contacts to create a very long, contorted arc with high-voltage and a high tendency to quench. The blast also cools and further constricts the arc. Explosive switches use a redundant number of explosive charges and small arcs with a moderately high voltage in each arc. Both types of switch can also be counterpulsed to increase the probability of current interruption. However, even in a forced-current zero circuit with no capacitor, an inductor is still needed as a snubber, in order to limit the dV/dt rise across the superconducting magnet, as discussed next.

Interrupters. In order to protect a superconducting magnet with an external dump resistor, an absolutely reliable current interruption switch is needed. Several current interruption switches have been used in magnet design for quench dump or other high voltage pulses. Whatever technology is selected, the interrupters will usually have two opening switches in series in order to provide adequate reliability. The dump strategy will then be either to open both series switches at once or to detect a failure to open in a nondestructive opening switch (e.g., a solid-state switch), then to open a more reliable but destructive switch (e.g., a series explosive switch). An interrupter may also include a switch to shunt conductor current during normal operations in order to reduce the steady-state ampacity requirement of the main interrupter. In this case, the high-current, inexpensive, normally closed mechanical switch transfers current into the quench dump interrupter after quench detection. The interrupter then carries the magnet current only as long as is needed to open and transfer its current to the external dump resistor.

Interrupting switch technologies include:

1. Thyristor breakers with counterpulse circuits
2. Mechanical breaker (air, air blast, vacuum, vacuum and magnetic field)
3. Explosively actuated breaker (fuse and fuseless)
4. Water cooled fuses (activated by water flow interruption)
5. Gate turn off (GTO) thyristor breaker
6. Insulated gate bipolar transistor (IGBT) switches
7. Superconducting switches

Turn-on switches that are used for the counterpulse circuit include:

1. Ignitrons
2. Thyristors
3. Vacuum switches

In the past, mechanical interrupters were favored for large magnets, because of the high power handling capabilities of a single device (e.g., up to 73 kA × 24 kV in the JET air-blast interrupter (2). However, with mechanical interrupters, the inevitable electrode erosion by current interruption arcs tends to limit the number of reliable operations to $\sim 10^4$ operations with periodic maintenance every 10^3 interruptions. The probability of failure (to interrupt current) in a mechanical interrupter has also been typically 10^{-3} to 10^{-4} at best, although this is clearly dependent on the specific design. For example, Yokota reported vacuum bottle tests in which there were five interruption failures in 10,000 interruptions with single bottles and no failures in 10,000 with two seriesed bottles (3). Clearly, any degree of reliability can be achieved with mechanical switches with adequate redundancy and maintenance. However, high-reliability requirements are usually met by the use of solid-state devices. Because they have no moving parts and are erosion-free, their lifetimes can easily exceed 10^6 operations, limited only by thermal fatigue. While individual solid-state devices used to be limited to the range of 1 kV × 1 kA, it is now possible to purchase thyristors with ratings of 6 kA × 6 kV. In the case of thyristor solid-state switches, the reliability of interruption will probably be set by the counterpulse circuit with the failure mechanism being either capacitor burnout or failure to close of the counterpulse circuit switch. The counterpulse circuit and its reliability limitations can be eliminated by the use of GTOs. They have always had less power-switching capability than normal thyristors, but are currently available with ratings of 3.3 kV × (4 kA, turn-off, 1.2 kA, ss). A new technology, IGBTs, is beginning to be used in high-power applications requiring fast switching, with device ratings up to 3 kV × (1.2 kA, turn off × 400 A, ss). IGBTs can be switched an order of magnitude faster than conventional thyristors, making them useful in switching converters that reduce the amount of filtering or voltage ripple on the magnets.

Explosive fuses are now capable of operating with very high reliability. They are inexpensive and incorporate redundancy in a single unit by including several in series explosive charges and arcs. They are frequently counterpulsed for further redundancy. Explosive fuses have the particular problem that they won't interrupt currents below a certain level. They are therefore most appropriately used in quasi-steady-state operations, in which low current quench is highly unlikely, or in those magnets that can guarantee passive internal absorption of the quench energy. They also favor applications where quench is highly unlikely, because they can only be used once.

A clever hybrid was proposed by Kuchinski to minimize the total cost of mechanical and solid-state interrupters (4),

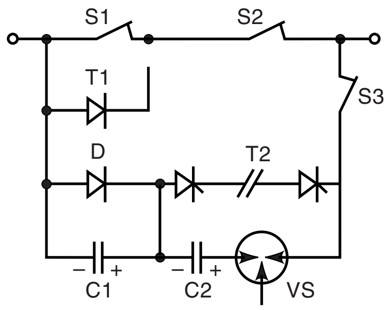

Figure 4. An arc-free current interrupter with pulse-rated solid-state components.

as shown in Fig. 4. This circuit allows all of the solid-state components to be pulse rated, while eliminating arcing in all of the mechanical components. S1 and S2, low-voltage mechanical switches, carry the magnet operating current. To interrupt, the thyristor T1 fires, suppressing any arcs, while S1 opens. T2 fires to initiate the counterpulse through T1 that turns it off. With D and T2 carrying magnet current with a low voltage drop, S2 opens. Then the vacuum switch is ignited to provide the reverse counterpulse through T2 to switch it off. All switches are interrupted and magnet current flows through the dump resistor.

Dump Resistors. The most common dump resistor is a meander of steel bars. Alternative dump resistor concepts include:

Dump Resistor	Advantages
Steel bars in air	Simplicity, cost, maintainability
Steel bars or ribbon in water (5)	Simplicity, energy density
Liquid rheostats (6)	Energy density, elimination of solid structure; Disadvantage: negative temperature coefficient
Voltage clamps (Zeners, MOVs, ZnO)	Faster dump for fixed peak voltage; Disadvantage: High cost/Joule

The voltage across a linear resistor declines with the current. Since electrical integrity is limited by voltage, it would be more efficient to use a resistor that discharged at constant voltage. With a perfect voltage source, either the peak dump voltage could be lowered by one-third or the dump time could be improved one and a half times. This can be approximated by highly nonlinear resistors, such as Zener diodes, Metal Oxide Varistors (MOVs) or Zinc Oxide (ZnO) arresters (7). At very high energy levels, these are prohibitively expensive. An inexpensive alternative with a useful degree of nonlinearity is stainless steel, which has a resistance temperature coefficient of ~0.001/K. If the temperature of a stainless steel resistor is allowed to rise 500 K by the end of a dump, its resistance will have increased by 50%. With nickel–iron alloys, the resistance can be quadrupled by the end of a pulse (1).

External Quench of Multiple Magnets. Both magnets and switches are limited in voltage and current. When a magnet system becomes too large, the dump circuit must subdivide into several parallel, series, or independent circuits. A particularly elegant circuit topology is that of the series interleaf, used in the tokamak systems T-15 and the Tokamak Fusion Test Reactor (TFTR), a normal magnet system. The series interleaf connection is shown in Fig. 5 (8).

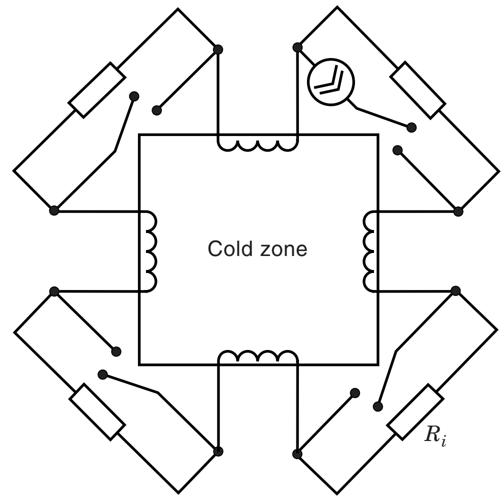

Figure 5. Series interleaf protection circuits [Dudarev et al. (8)].

This circuit has two advantages over independent or parallel protection circuits. With the interleaf, the voltage drops alternatively up and down, because of the alternation of superconducting inductors and external resistors, as shown in Fig. 6. This prevents high voltage from building up through the coil system, as it would do if there was only a single dump resistor. If the large coil system had simply been broken into the same number of independent or parallel dump circuits, there would be a possibility of unbalanced currents and forces, during a quench dump. With a floating power supply, the interleaf circuit also prevents unbalanced forces during a single ground fault.

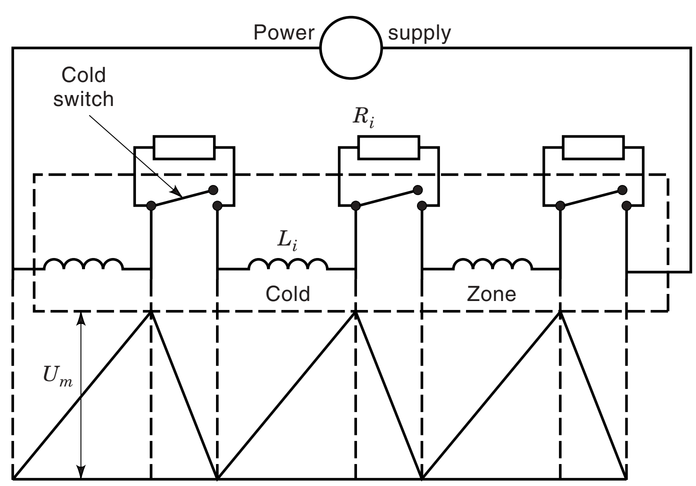

Figure 6. Series interleaf circuit dump waveform [Dudarev et al. (8)].

Alternative options for dumping energy in a mutually coupled multicoil system are summarized in the table.

Dump Strategy	Advantages	Disadvantages
Dump all coils in series	Simplicity, no unbalanced currents or forces even with single ground fault	High terminal voltage
Dump all coil in series interleaf	No unbalanced currents or forces even with single ground fault; low voltage	As many VCLs and dump circuits as interleafs
Dump all coils in parallel; dump all coils independently	Low voltage; independent control	Possibility of unbalanced currents and forces; large number of VCLs; least reliable for given component reliability
Dump faulted coil externally; other coils remain in persistent mode (ORNL EPR)	Smallest refrigeration requirement for recool	Overcurrents in persistent magnets when coupled to dump coil

Internal Dump

Magnets are dumped internally when it is desirable to eliminate helium loss through the vapor-cooled leads and when terminal voltages have to be severely limited, as with commercial products, such as MRI magnets, where users have to be in the same room as the magnet. The least aggressive action that is typically taken with a pool-boiling magnet is simply to disconnect the superconducting coil from the power-supply and allow its current to die down slowly as it freewheels through a superconducting switch or normal joint. This would be an appropriate response to a low liquid-level reading, in which an active dump might do more harm than good.

Cold dump resistors may still be either internal or external to the magnet. That is, a large fraction of the energy can be deposited into resistors or diodes that are outside of the magnet, but inside the cryostat. However, since there is now no benefit in refrigeration or cooldown requirements in removing energy from the magnet, it is almost always desirable to return as much of the heat as possible to the magnet, thereby creating longer quench zones and more uniform heat deposition with the magnet. This can be done by making the resistive element a heater, closely coupled to the outer layer of the magnet or cowound with the magnet superconductor.

Cold Dump Circuits. In a cold dump circuit, either the interrupter or the resistor or both will be inside the cryostat at the magnet temperature. Cold switches include superconducting switches and fuses, cold diodes, and cold transistors. Cold resistors include cowound, insulated normal metal, surface heaters, and power dissipation in the switch itself. One benefit of having all elements of the dump circuit cold, when the switch is superconducting, is that the vapor-cooled leads can be detached, allowing current to circulate losslessly in the magnet. Cold heaters have two additional benefits, especially when they are cowound through the entire magnet. They can prevent hot spots by reducing the peak local/average heating, and they can also cancel the dI/dt voltage of the magnet with the resistive voltage, greatly reducing internal voltages in the coil. Both the thermal peaking factor and the internal voltage can be reduced by orders of magnitude from the external dump option in a well-designed internal dump circuit.

The disadvantage of a cold resistor is that all of the magnet energy is absorbed at cryogenic temperature, greatly increasing the time and cost for recool. Therefore, strings of accelerator magnets, which involve a very large number of magnets and training (see SUPERCONDUCTORS, STABILITY IN FORCED FLOW) quenches, use cold switches, but dump externally in order to achieve a large number of rapid cooldowns. CICC magnets and absolutely stable pool-boiling magnets are not supposed to quench. If they do, the engineering postmortem would generally take more time than cooldown, and recool is not a major consideration. The disadvantage of a cold switch is that the power-handling capability of an individual switch is much smaller than that of a warm switch. Above approximately 200 V $\times$ 15 kA, cold-switching becomes impractical.

Cold switches can be triggered actively or passively. Cold diodes begin to conduct when a forward voltage higher than a threshold is applied. Cold transistors begin to conduct when a forward voltage higher than the turn-on voltage is applied to their base. The transistor gain allows them to be over an order of magnitude more sensitive than the diodes. Superconducting switches can be driven normal by external heaters or induction coils, coupled closely with the switch. These triggers may either be driven from a small, external power supply, or be driven passively by the magnetic induction of the quench itself.

A fully actively driven resistor doesn't actually require any switch. Usually, the entire magnet can be driven normal, by applying heat that is less than 1–2% of the magnet stored energy. A small external circuit can drive the current in a cowound resistor or a heating pad on the outer layer in order to ensure a large quench zone. A totally nonresistive method for creating a long quench in a large coil has also been proposed, in which helium would be rapidly drained from the cryostat (9). Advantages and disadvantages of each method are listed in the table.

Cold Dump Circuit	Advantages	Disadvantages
Metal strips	Low $/kg; uniform heating easy	Extremely massive, bulky
Superconducting switches	Ideal for low energy coils with persistent currents	Much too expensive for large coils; both massive and high $/kg
Superconducting fuses	Can develop higher voltage, faster dump than superconducting switches	Much too expensive for large coils
Internal resistive heaters	Guarantee uniform heating of coil, without imposing high quench propagation velocities. High degree of redundancy can be designed in. No bulky dump structures outside coil	Extraction of leads from CICC must be leak-tight, resistive drop must be low enough to prevent arcing within sensor
Fast helium drain to induce global quench	No bulky dump structures outside coil	Slower, less uniform heating of coil than resistive heater. Not applicable to CICC

It is our opinion that cowound, resistive heaters have the fewest theoretical limits in almost all cases. They will always

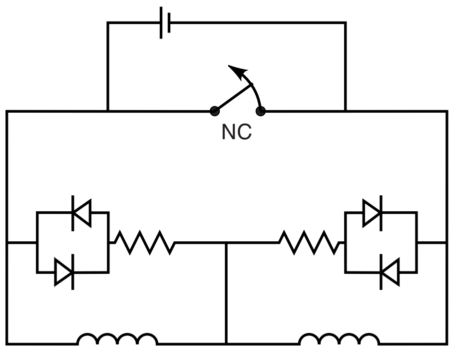

Figure 7. A representative dump circuit using cold diodes.

achieve the least peaking in energy deposition and internal voltage. They can also be used in all applications as advanced quench detection sensors, as discussed below; and they can sometimes be used as structural backing elements.

Cold Switches. A typical cold switch is shown in Fig. 7. Here, by splitting a coil into two halves it is possible to apply a resistive dump voltage to both sides without opening the normally closed switch across the coil as a whole.

In this circuit, the magnets are charged through the power supply, which is then shunted through the normally closed switch, allowing current to circulate through the magnets. If a quench begins in either half of the center-tapped coil, the voltage across the switch is zero, but the inductive voltage on the unquenched half is equal and opposite to the inductive and resistive voltage across the quenched half. Above the cold diode threshold of 10 V to 15 V, two of the four diodes begin conducting. The resistor is sized so that its voltage drop is much larger than the 1 V to 1.5 V forward drop across the diode, but small enough to satisfy Underwriter Laboratory safety limits, typically 100 V. The resistor itself might be a heater pad on the outer layer of the winding, inducing a longer quench zone and more uniform heat distribution in the coil.

In the circuit shown in Fig. 8, cold transistors are used, instead of cold diodes, in order to block high voltages during both charging and discharging of the magnet system. Kaerner (10) found that the only active devices blocking bipolar voltages at helium temperatures are NPT (non-punchthrough) IGBTs (Insulated Gate Bipolar Transistors). In 1995, a single device would carry 300 A at 5.9 K and block 1200 V. In this system, after quench is detected, the "weak" coil is shunted by the IGBT, the coil is rapidly dumped by internal heaters, then the rest of the coils are ramped down. With this scheme, only $1/n$ coils of the stored energy has to be dumped at helium temperatures, but there is only one set of vapor-cooled leads.

Probably the most commonly used cold switch is a normally closed superconducting switch. During coil charging, it is held normal by an actively driven heater. The heater is then turned off and frequently the charging leads are then disconnected to reduce losses. These can be used in conjunction with a cold transformer in order to lower the voltage threshold for passive dumping. Anashkin et al. designed a passive circuit that is capable of responding to very low rates of current decay (11). The circuit in Fig. 9 demonstrated a superconducting switch normal transition for a magnet field decay of 2×10^{-4} T/s.

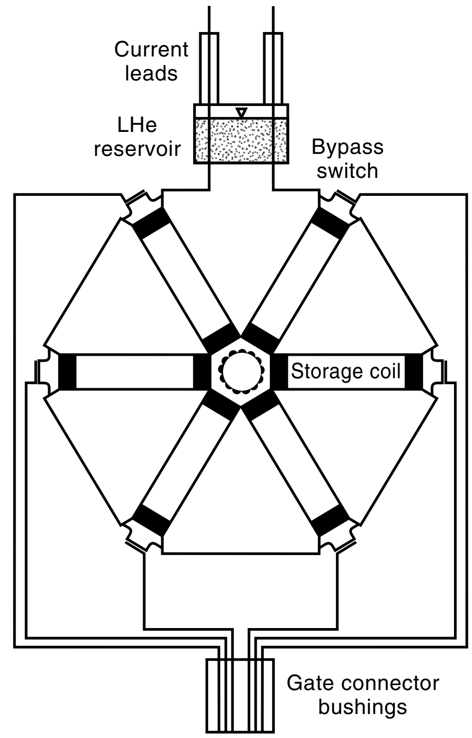

Figure 8. Arrangement of cold bypass switches in toroidal SMES system [Kaerner et al. (10)].

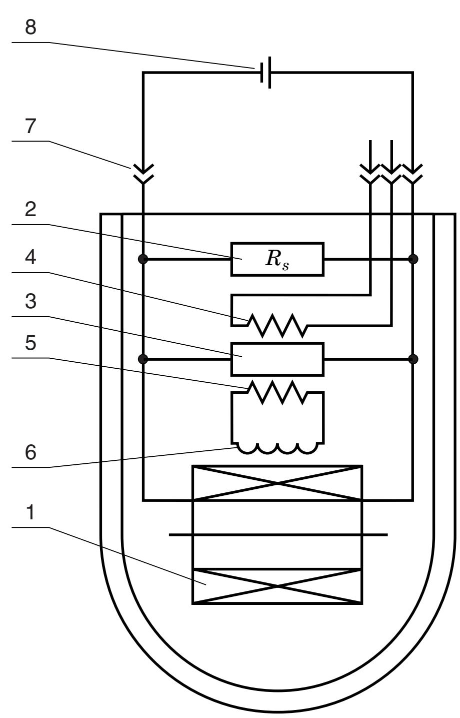

Figure 9. Highly sensitive passive protection circuit: (1) Superconducting magnet, (2) Shunt resistor, (3) Superconducting switch, (4) Main switch heater, (5) Auxiliary switch heater, (6) Secondary winding, (7) Detachable current leads, (8) Current supply [Anashkin et al. (11)].

The current decay due to a normal zone induces current in the secondary winding and auxiliary heater which drives the superconducting switch normal. Most of the magnet current is now forced through the shunt resistor. The shunt resistor can be placed either inside or outside the cryostat. An external resistor would be favored for applications with a large number of magnets or expected training quenches, such as accelerator rings, in which cooldown time and refrigeration requirement dominate. Internal placement is favored for very high performance magnets, where the resistor can also be used as a magnet heater to force uniform quench.

QUENCH DETECTION

Superconducting magnets have traditionally used relatively simple methods for detecting a quench. Voltage taps on the surface of a winding are the most common, and changes in temperature, pressure, and flow have also been used, sometimes as supplements to voltage taps. These methods become inadequate when a magnet has to operate in a strongly pulsed field. The problem of induced noise voltage is exacerbated by large size and large transients in flow or temperature. In the future of large commercial systems, requiring high reliability, quench detection is likely to be the weak link in the magnet protection system. While series redundancy can provide arbitrarily high reliability in external protection circuits, it will require advanced concepts to guarantee high signal-noise ratio, rapid detection, along with leak-free and discharge-free quench detection under all operating conditions.

Voltage Sensors

Conventional Voltage-Taps and Bridges. The voltage across a coil or a section of a coil is measured by tapping into the external surface of the conductor through the insulation. This is commonly done at sections of the winding pack that are physically close to each other, in order to avoid unnecessary inductive pickup, but which may still have significant voltages between them, such as the voltage across two layers or two pancakes. This method, being the crudest and most likely to be overwhelmed by inductive noise, is used with very slow-charging dc magnets. The signal-noise ratio of voltage taps is most frequently enhanced by the use of a bridge circuit to cancel out the inductive signal. Two nearly equal inductive signals, such as the inductance of two adjacent double pancakes or an external inductance with the same or proportional dI/dt as the coil are put in two arms of the bridge. An external resistance is then balanced against the coil section whose resistance is being measured, and the ramped superconductor signal is zeroed out. Any voltage should then be equal to the resistive drop across the magnet during a quench. A typical bridge circuit design by Purcell (12) is shown in Fig. 10.

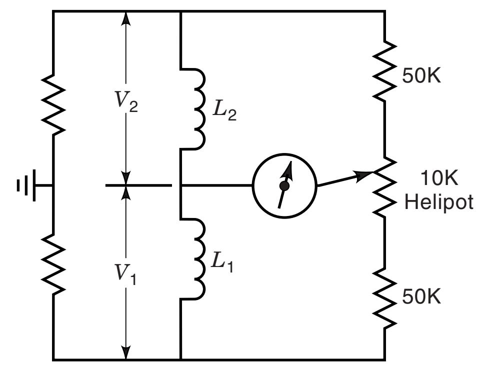

Figure 10. Quench detection bridge circuit [Purcell et al. (12)].

Pick-Up Coils. If a coil is connected to a low transient impedance external circuit, it is possible to detect a quench by inductive pickups to an overall magnet change in current. An external dump circuit can then be triggered to accelerate the coil dump. A typical use of a pickup coil quench detector by Sutter (13) is shown in Fig. 11.

A variation on this technique is to place higher-order pickup coils around a superconductor as a multipole antenna (14). During a quench, circulating supercurrents will be suppressed more rapidly than overall current, causing a rapid collapse of diamagnetism in the conductor that can be detected by the antenna. Both techniques have the advantage of not interrupting the coil insulation.

Detection Circuits. The basic detection circuit by St. Lorant (15), shown in Fig. 12, would trigger a quench dump, based on a resistive voltage level that exceeds a preset threshold, typically 10 mV to 200 mV. In a bridge circuit, resistive voltages of either polarity must be expected. Low-pass filters prevent false positive signals due to ambient noise. The comparator is the quench detector itself. The rectifier allows either positive or negative voltages to be used as unipolar digital triggers. A signal inhibit may be used to prevent quench triggers during coil ramping, and the Schmidt trigger creates a trigger pulse of fixed amplitude and duration.

Advanced Detection Techniques

In a large magnet, the terminal voltage during pulsing may be as high as 5 kV to 25 kV. The POLO coil set a world's record for CICC at 23 kV (16), while recent designs of large CICC coil systems, such as ITER (10 kV), TPX (7.5 kV), and NAVY SMES (10 kV) have specified voltages in this range, while the important pool-boiling Anchorage SMES system is being designed to withstand 4.2 kV. By contrast, a large number of quench simulations have shown that in order to hold hot-spot temperatures to 150 K, a quench must be detected at a threshold voltage of 0.2 V to 1.0 V (17,18). If, as in the TPX design (19), a desired value of signal/noise of 10 : 1 is specified, the quench detection sensors must be capable of reducing noise levels to ~20 mV to 100 mV. This implies that the voltage rejection capability of the quench detection system should be on the order of 100,000–500,000 : 1. Although this may seem optimistic, recent experiments at MIT, the Lawrence Livermore Laboratory, and the Ecole Polytechnique Federale de Lausanne have demonstrated the feasibility of such high levels of voltage noise rejection (17,20).

New techniques that promise the greatest cancellation of inductive noise and the highest signal/noise ratios include the use of internal sensors, digital differencing and signal processing, and fiberoptic temperature sensors.

Advanced Voltage Sensors. Several noise rejection techniques can be used simultaneously in order to obtain ultra-

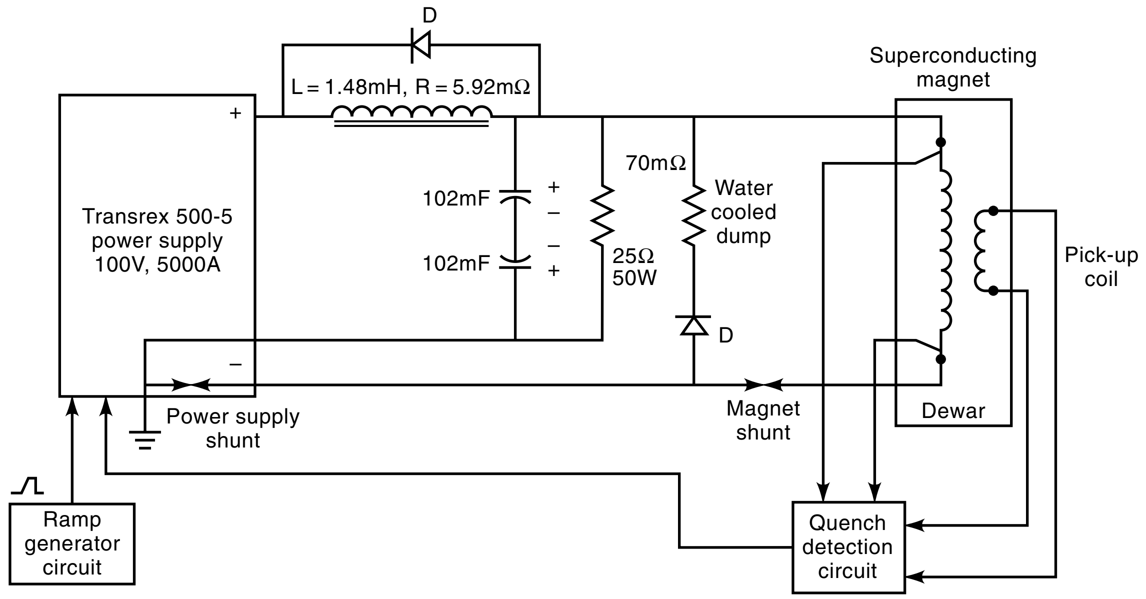

Figure 11. Use of pickup coil quench detector in the Fermi National Accelerator Laboratory's energy doubler magnet [D. F. Sutter et al. (13)].

high system noise rejection. Individual concepts that can be used include:

1. Cowinding an insulated voltage sensor with the CICC cable
2. Extracting voltage sensors at joints, but terminating them within the winding; thus subdividing the terminal voltages and localizing quench information, without exacerbating electrical integrity or leak tightness
3. Placing the cowound sensor in the part of the cable best calculated to reject transverse, longitudinal, and self-field voltages. Placement of voltage taps in the center of the final stage subcable was favored by TPX, as shown in Fig. 13 (17)
4. Terminating the voltage sensor internally, further localizing and subdividing the winding into sections, and permitting another level of voltage differencing, such as simple differencing and central difference averaging. The two halves of the sensor form one solid wire that can be cabled and wound with the rest of the conductor. A method for forming an internal termination in a continuous sensor is shown in Fig. 14
5. Further signal processing, such as using integrated volt-seconds, rather than simple voltage thresholds as detection criteria

These techniques are now described in more detail.

Cowinding an Insulated Voltage Sensor with the CICC Cable. A cowound sensor has been used previously on the US-Dual-Purpose Coil (US-DPC) coil, where an insulated wire was wound along an edge of the conduit on the outside (21). A cowound, insulated aluminum strip in the B&W SMES coil is

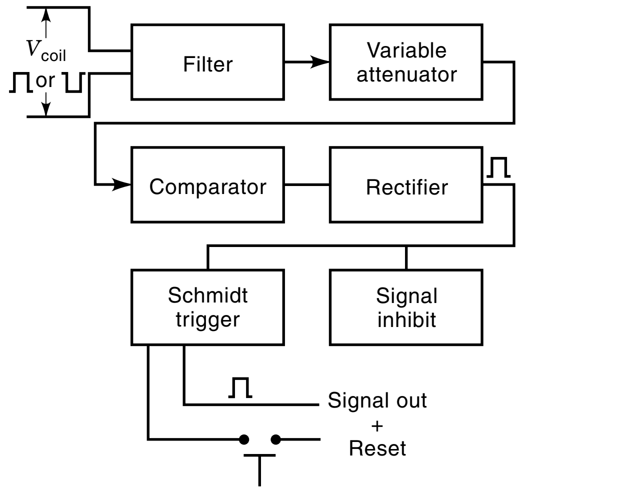

Figure 12. Basic quench detection circuit block diagram [S. J. St. Lorant et al. (15)].

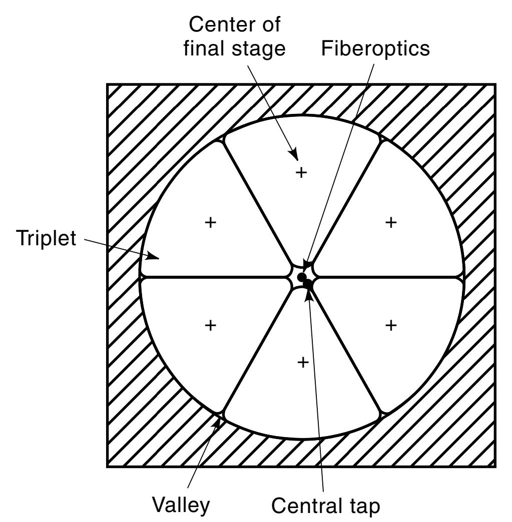

Figure 13. Placement of sensors within cable.

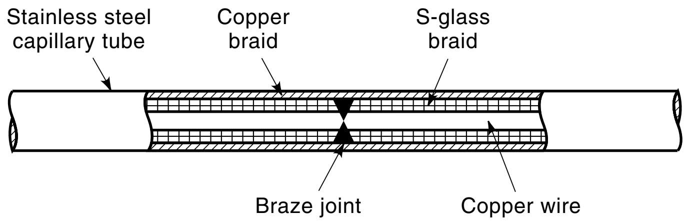

Figure 14. Two-sided voltage sensor, showing internal termination between two halves.

also being used as structural reinforcement. If the sensor is cabled on the inside of the conduit, as shown in Fig. 13, the degree of noise cancellation will improve by at least another order of magnitude. The ITER QUELL (Quench on Long Lengths) experiment demonstrated the cabling and extraction of voltage sensors on the surface of a cable, but inside the conduit, for a 100 m length of conductor. In the QUELL experiment, the rejection of transverse voltage was more than 400 times better than that of conventional voltage taps (21). Two TPX experiments, one with a copper cable, the other with a NbTi cable, demonstrated cabling of sensors in different positions of a full-scale cable (17). Depending on the sensor position, noise rejection ranged from 600–60,000 : 1.

Extracting Voltage Sensors at Joints. Joint extraction from the ends of a continuous winding, while difficult, is much less intrusive than extraction every two layers or pancakes through the winding pack. The joints must already be accessible for servicing and capable of accommodating helium stubs and lines and instrumentation feedthroughs. The biggest problem with extracting voltage sensors at the joints is ensuring that they will not leak helium and that they won't be subject to electrical breakdown. The approach to preventing leaks is two-fold: (1) injecting a moderately sized seal area with a mineral-filled sealant, such as Stycast, with a good thermal match to the seal metal, and (2) designing the seal to be long, in compression, and mechanically redundant in terms of interrupting individual microcracks, and (3) made up of a separate, weldable piece that can be thermal shock tested or cycled before installation. A simple version of this joint was demonstrated at MIT that, after two cooldowns to nitrogen, was capable of holding 70 bars on one side and vacuum on the other (17).

Design against electrical breakdown is ensured by designing the CICC itself, so that there can never be 160 V across the voltage sensor. In this case, the sensor insulation will be below the Paschen minimum for helium, irrespective of uncertainties in helium pressure due to leaks or in stray transverse or longitudinal magnetic fields. Almost any large magnet will satisfy this design approach automatically. For example, a normal zone as long as 1 km with a stabilizer current density of 200 A/m^2 at an average field as high as 13 T, would have a resistive voltage of only 133 V between joints. Depending on the time needed for internal current dump, the current density can be lowered slightly, if needed, in order to compensate for resistivity rising with temperature. This should seldom be necessary.

Placing the Cowound Sensor in the Part of the Cable Best Calculated to Reject Transverse, Longitudinal, and Self-Field Voltages. The surface of the cable is not the best position for emulating the trajectory and therefore the flux linkage of a typical strand in a cable. The best job would be done by a sensor that was cabled into a first triplet, as though it were a strand. The second best position, identified so far, is to place the sensor in the center of the final stage of the cable, which is easier to cable and not vulnerable to conduit broaching or welding. Both positions are far superior to the center of the cable or a natural cabling valley on its surface. Equations for approximating the induced noise voltage for different types of field and sensor placement were derived by Martovetsky (22) and are summarized in Table 1.

Terminating the Voltage Sensor Internally. Internal termination of sensors localizes the signal by subdividing the winding into sections and permits another level of voltage differencing, such as simple differencing and central difference averaging. In TPX, the voltage sensors were terminated internally at 1/6, 1/3, 1/2, 2/3, 5/6, and completion of the distance through the winding pack, as shown in Fig. 15. Even before using differencing techniques, this should further reduce the noise voltage by another factor of six, in a way similar to putting voltage taps on each one of six double pancakes. Taking a simple difference between, say, the signal at 1/6 and 1/3 is frequently ineffective, since there may be a systematic gradient through the winding pack due to eddy currents being turned around by a break on one side of the winding pack, but not the other (23). However, central difference averaging, in which one-half the first and third sensor signal are subtracted from the middle sensor, as first proposed by Yeh and Shen (24), can be effective in canceling out gradients. For example, if voltages are measured across double pancakes, the threshold voltage across the first six pancakes would then be $0.5V_{1-2} - V_{3-4} + 0.5V_{5-6}$. In simulations of TPX, the degree of further cancellation using CDA was 5–20 (17). Internal termination has the additional benefit of localizing quench initiation and of following the sequence of quench propagation through a winding pack.

Using a sensor insulation that is compatible with inexpensive seam-welding of the steel capillary tube permits the redundant use of multiple voltage sensors in a cable. Fabrication of sensors with S-glass braid, as shown in Fig. 16, was demonstrated in the QUELL experiment and the ITER CS Model Coil. Some combination of Formvar, teflon, and/or kapton would be used for NbTi. Teflon would probably be most desirable, because of its ability to eliminate seams at modest temperature and pressure, thus eliminating tracking. XMPI Kapton, at higher temperature and pressure, should have even higher performance.

Further Signal Processing, Such as Using Integrated Volt-Seconds, Rather Than Simple Voltage Thresholds as Detection Criteria. This is particularly effective in screening out short disturbances, such as stick-slip, flux jumps, and plasma disruptions. In TPX simulations, an additional factor of 10–20 in signal/noise was achieved by using a volt-second window, instead of a voltage threshold (17). Further improvements in signal/noise ratio through signal processing have been proposed through the use of carrier signals and synchronous detectors.

In summary, although there is clearly a broad range of design specific signals and signal/noise ratios, the following rules of thumb might be used for preconceptual design of a voltage noise reduction system with the goals of achieving a signal/noise level improvement of $>10^5$ (i.e., 10 kV down to 100 mV): Split the winding pack into sections (5–10) $\times$ Place

Table 1. Noise Voltages for Different Sensor Positions

	Transverse Field	Self Field	Parallel Field
Wire in center	Grad-*B* $V = \frac{1}{2}\int_0^L \frac{\partial \dot{B}_z}{\partial r} r^2_{\text{last stage}}\, dl$ Geometry $V = \dot{B}\frac{N_{\text{turns}}\, d^2_{\text{cable}}}{2}$	$V = \frac{\mu \dot{I} r^2}{4\pi R^2} L$	$V = \int_0^L \dot{B}_\parallel \sum_{n=1}^{4} \frac{\pi r^2_{\text{subcable},\,n}}{l_{p,n}}\, dl$
Wire in valley	Grad-*B* $V = \frac{1}{2}\int_0^L \frac{\partial \dot{B}_z}{\partial r} r^2_{\text{last stage}}\, dl$ Geometry $V = f(\text{Inhom}) \times \frac{1}{2\pi}\int_0^L \dot{B}_z r_{\text{cable}}\, dl$	$V = \frac{\mu \dot{I} L}{4\pi} - \frac{\mu \dot{I} L}{12\pi}$	$V = \int_0^L \dot{B}_\parallel \left(\sum_{n=1}^{4} \frac{\pi r^2_{\text{subcable},n}}{l_{p,n}} \frac{\pi r^2_{\text{cable}}}{l_{p,cable}} \right) dl$
Wire in triplet	Grad-*B* $V = \frac{1}{2}\int_0^L \frac{\partial \dot{B}_z}{\partial r} r^2_{\text{last stage}}\, dl$ Geometry $V = f(\text{Inhom}) \times \frac{1}{2\pi}\int_0^L \dot{B}_z r_{\text{last stage}}\, dl$	$V = f(\text{Inhom}) \times \frac{\mu \dot{I} L}{12\pi}$	$V = f(\text{Inhom}) \int_0^L \dot{B}_\parallel \sum_{n=1}^{4} \frac{\pi r^2_{\text{subcable},n}}{l_{p,n}}\, dl$
Wire in center of final stage	Grad-*B* $V = \frac{1}{2}\int_0^L \frac{\partial \dot{B}_z}{\partial r} r^2_{\text{last stage}}\, dl$ Geometry $V = f(\text{Inhom}) \times \frac{1}{2\pi}\int_0^L \dot{B}_z r_{\text{last stage}}\, dl$	$V = \left(\frac{\mu \dot{I} L}{12\pi} - \frac{\mu \dot{I} L}{16\pi} \right)$	$V = \int_0^L \dot{B}_\parallel \sum_{n=1}^{3} \frac{\pi r^2_{\text{subcable},n}}{l_{p,n}}\, dl$

internal sensor in cable final stage (100–1000) × central difference average (5–10) × filter, integrate, signal process (5–10) = 10^4–10^6. Two TPX noise injection experiments, one with copper, the other with NbTi cable, demonstrated transverse field noise rejections of up to 60,000 (17). The ITER QUELL coil had both conventional and cowound voltage taps on the outside of the cable in its natural valleys. In this experiment, the voltage rejection of the cowound sensor was 80 times better than that of the noninductive winding with a voltage rejection of 6 : 1 or 500 : 1 total. Another noise-rejection method used in ITER of differencing multiple in-hand windings was calculated to achieve noise rejection ratios of 300–400. A better way to normalize the results to design for all noise sources is to show that the V/(km-T/s) are $\ll 1$ for transverse field and $\ll 10$ for parallel and self-field, corresponding to $\ll 1$ V for 1 T/s over a kilometer. Placement of the sensor in the center of the final stage or in a triplet have, so far, met this goal in all experiments.

Advanced Fiberoptic Temperature Sensors. Conventional temperature sensors have a number of disadvantages: they cannot be inserted inside a cable-in-conduit, don't measure cable temperature directly, and have a significant time lag. Like conventional voltage taps, they can't give coverage to a winding without frequent penetration of the insulation system. Furthermore, thermocouples are insensitive at helium temperatures, while carbon glass resistors and resistance temperature detector (RTD) sensors are insensitive at quench temperatures. The use of fiber optic temperature sensors, protected by a steel capillary, as shown in Fig. 17, has several advantages over conventional sensors: (1) They can be inserted directly into the helium flow channel with a very short

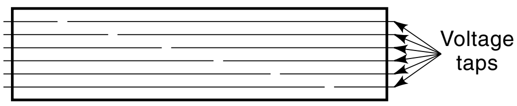

Figure 15. Inexpensive voltage sensor concept.

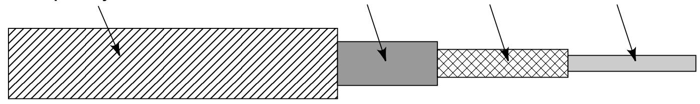

Figure 16. Six internal voltage sensors, terminated at equal distances through cable.

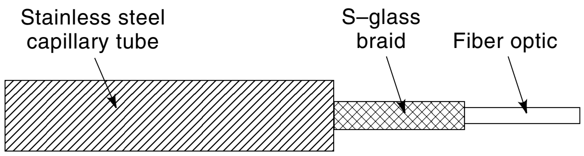

Figure 17. Fiber-optic sensor.

thermal time constant, (2) they are insensitive to pulsed magnetic fields (25), helium flow, and pressure, (3) they are very small (<50 μm), so as many fibers as desired can be placed in a single steel can, (4) the length of a fiber between joints is practically unlimited, 50 km being a routine commercial length, and (5) they have great scientific potential in the use of signal processing to provide a complete profile of temperature and field versus length and time.

Fiberoptic temperature sensing works on the principle of measuring optical path length, taking advantage of the temperature dependence of the glass index of refraction. The change in phase from either effect is

$$\Delta\varphi = \frac{2\pi}{\lambda}[n\Delta L + \Delta n L] \tag{2}$$

where $\Delta\phi$ is the phase shift and n is the index of refraction.

The major problem with this technique is the rejection of path length changes due to mechanical strain in the glass. One strain-rejection technique is to decouple the glass from the conduit containing it, so that they don't share strain. At M.I.T., a fiber was inserted in a 1.0 mm stainless steel capillary tube and several turns were wound on an 80 mm steel tube. The assembly was heated to 700°C, then cooled to 4 K without damage, thus demonstrating strain decoupling and the absence of a capstan multiplying effect on fiber tension (26). The QUELL experiment demonstrated that the relatively loose fit of a copper-clad fiber can reduce the strain-sharing by a factor of 10–100. However, mechanical strain was still a dominant effect, since the changes in index of refraction are <1%. It has been demonstrated by Smith that the mechanical strain and temperature-dependent signals can be almost totally decoupled by using two independent signals with different strain and temperature dependences (27). This can be accomplished by the use of polarization maintaining (PM) optical fiber, two color operation, or two mode operation. Each polarity, color, or mode has a different, calibrated ratio of strain and temperature dependence, so that the gain on one phase shift can be adjusted to 'tune out' the strain signal. This method has the additional benefit that it can also be used to measure the integrated conductor strain. Overall system cost-performance analysis indicates that two mode operation will probably be the most cost-effective long-term solution. Typical sensitivities are shown in Table 2.

Table 2. Sensitivity of Dual-Mode and Dual-Polarity Fiber to Temperature and Strain

Method	Temperature Sensitivity (radians/m-K)	Strain Sensitivity (radians/m-ε)
2 Polarities	1.2	5×10^3
2 Modes	2.18	55×10^3
2 Colors	0.1	0.5×10^3

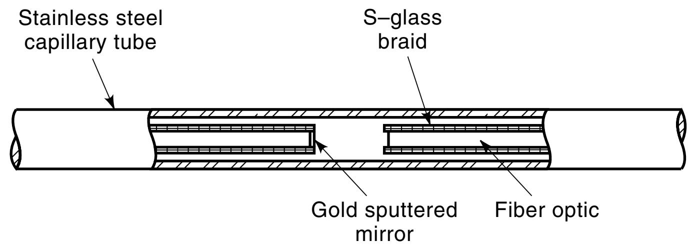

Figure 18. Internal termination of fiber optic temperature sensor.

Glass-fiber must be clad in order to prevent the entrance of water during handling. Commercial acrylic fibers are adequate for NbTi, but will not survive Nb_3Sn, NbAl, or BSSCO heat treatments at >600°C. Although the surrounding steel can contain any spattering of the cladding, this solution is, at best, messy. Coatings of copper, gold, or graphite can protect the glass fiber and survive heat treatments. Unjacketed acrylic coatings should be used outside of the joint region, so that high-voltage cryostat feedthroughs won't be necessary.

The same design principles of internal termination applied to voltage sensors within a winding pack apply to fiber optic temperature sensors. If they are internally terminated by sputtering mirrors on polished cuts, as shown in Fig. 18, the integrated noise temperatures are reduced by the number of subdivisions, then reduced further by differencing techniques.

Subdivision also allows greater localization of quench events. In the special case of irradiated magnets, it also helps keep the signal attenuation manageable (<60 dB). The method for subdividing a fiber is to cut the fiber at the desired length, polish and silver the end. The fiber end is then a mirror and the laser light signal returns to the splitter and detector to form the information-carrying half of a Michelson interferometer.

After converting phase shifts to voltages, the same signal processing concepts used for voltage sensors can also be used for fiber optics. Integrating the number of fringe shifts over a time window, such as one second, can achieve an order of magnitude improvement in signal-noise ratio. The signal-noise ratio of the fiber optic quench detector is naturally enhanced by the increase in sensitivity with rising temperature. Simulations of quench and disturbances in TPX showed minimum signal/noise ratios of 600 : 1 for quench detection within a second (26). This was both within design criteria and superior to internal voltage sensors. The temperature sensitivity of the fibers has been measured with and without cladding and can be characterized by an initial quadratically increasing fringe count according to the equation:

$$\int_5^T a\,dT = 1.75T^2 - 17.5T + 43.25;\ 5\text{K} < T < 9\text{K} \tag{3}$$

The increasing sensitivity saturates at about 15 fringes/m-K, and then only increases to about 25 fringes/m-K at room temperature, as shown in Fig. 19.

If the fiber optic sensor is considered to be a length-temperature rise integral measurement, the sensitivity is 200 times higher at 30 K than at 5 K. Therefore, a global disturbance that raises the helium temperature throughout a 1 km winding from 5 K to 5.2 K will give a signal that is smaller than a quench that raises 1 m of conductor to 30 K.

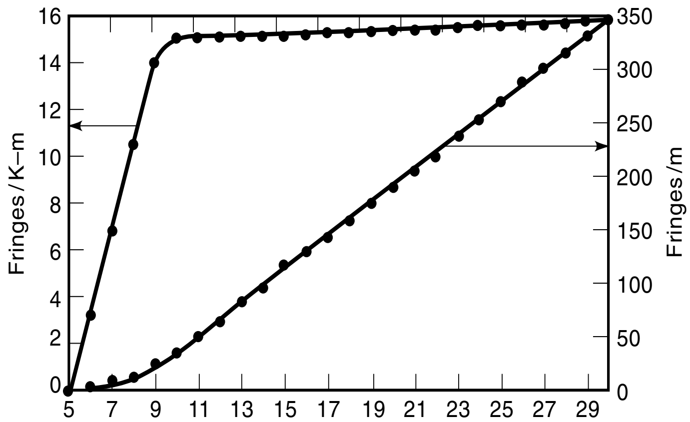

Figure 19. Temperature sensitivity of glass fibers.

For an unclad fiber, the sensitivity is almost exactly one-tenth that of a clad fiber, the thermal strain of the plastic cladding acting as an amplifier of the temperature signal. The curves in Fig. 19 can be used for design of temperature sensors with NbTi; but fringes/m-K should be multiplied by 0.1 for design with Nb_3Sn.

Fiber optic sensors would use the same sort of prefabricated and pretested seal as the voltage sensors. However, a few inches of clearance would be needed between a joint and the initial position of the seal piece, in order to use a hand-held field splicer. The optical fiber can then be coiled into the pocket of the seal piece.

Quench Detection Conclusions

1. Fiber optic temperature sensors and internal voltage sensors have been shown by simulation and experiment to improve signal/noise ratios in quench detection systems by several orders of magnitude.
2. A leak-free method for extracting sensors has been demonstrated, and a redundant and replaceable sealing system has been designed.
3. A method for coil/sensor electrical design has been defined that is robust against arbitrary helium pressures and magnetic fields. Enormous safety margins are feasible with NbTi and fused teflon or kapton insulation.
4. Advanced quench detection sensors can also be used as scientific instruments, measuring the internal properties of CICC conductors.

MAGNET PROTECTION CRITERIA

Adiabatic Protection Criterion

A popular and conservative protection criterion is to assume that there is no heat transfer from the local hot spot where quench is initiated and that all Joule heating is absorbed by the stabilizer. In this case, the relation between the peak allowable hot spot temperature and the J^2t integral of the conductor stabilizer during a coil dump is a unique property of the stabilizer material, usually copper. The maximum allowable current density is then determined by the peak allowable hot spot temperature and the peak allowable terminal voltage for a coil dump. Typical values of peak temperature allowables are 80 K to 200 K. If a coil is completely supported in compression by external structure, as an accelerator coil in a large iron yoke, it is possible to design up to 450 K or the melting point of solder (28). A typical allowable terminal voltage for a pool-boiling magnet is 1 kV to 3 kV, and 3 kV to 20 kV for a CICC magnet. However, as discussed in the section on electrical protection, the fundamental limits on voltage for both topologies are strong functions of specific design.

Irrespective of the coil temperature allowables, the selection of the peak terminal voltage fixes the minimum L/R dump time constant (s) at

$$\tau_D = \geq \frac{2W_m}{V_{\max} I_{\text{cond}}} \tag{4}$$

where W_m is the stored energy in the magnet (J), $V_{\max}$ is the peak allowable terminal voltage on dump (V), and I_{cond} is the conductor current (A). For a system dumping its energy into a linear external resistor with negligible resistive voltage within the coil system, the magnet current after switching is simply

$$I(t) = I_{op} \exp\left(-\frac{R_D t}{L_m}\right) \tag{5}$$

where R_d/L_m is the dump time constant τ (s).

Since a quench will not be detected immediately, there is also a delay time before any action is taken. This has sometimes been specified as 1–2 s as a design goal, but it is a function of the signal/noise ratio of the quench detection system, as explained in that section. The allowable current density in the copper then is fixed by the combination of delay plus dump time as

$$j_{0cu}^2 \left(t_{\text{delay}} + \frac{\tau_D}{2}\right) = Z(T_f) \tag{6}$$

where t_{delay} is the maximum possible time delay (s), T_f is the final temperature at the end of dump (K), and $G(T_f)$ or, alternatively in some texts $Z(T_f)$, is a property, unique to each material or combination of materials, defined as

$$Z(T_f) = \int_{T_b}^{T_f} \frac{C(T)}{\rho(T)}\, dT \tag{7}$$

This integral can also be thought of as the J^2t integral of the current in the conductor during a dump, and is thus usually represented with the units (A^2/m^4-s). An analytical approximation for $G(T_f)$ for copper from a bath temperature of 4.2 K is

$$Z(T_f) = \left(\frac{1363}{T_f + \dfrac{4173}{T_f + 47.89}}\right) \times 10^{16} \tag{8}$$

Another way of stating the design constraint, derived by Iwasa and Sinclair (29) defines $Z(T_f)$ as the integral from the detection temperature to the final temperature and models the presence of materials other than substrate by a correction factor a, which is the enthalpy change ratio of substrate/all other materials, which can be determined by table lookup or

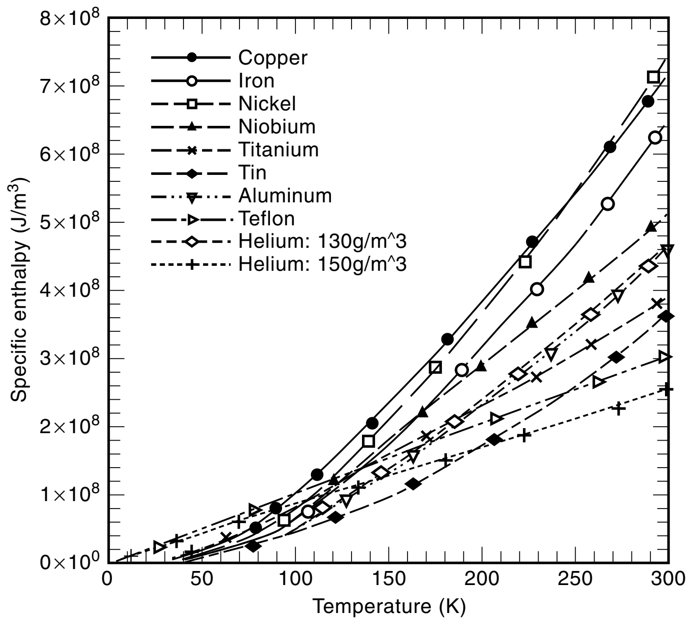

Figure 20. Specific enthalpies of magnet materials (J/m^3) versus temperature (K).

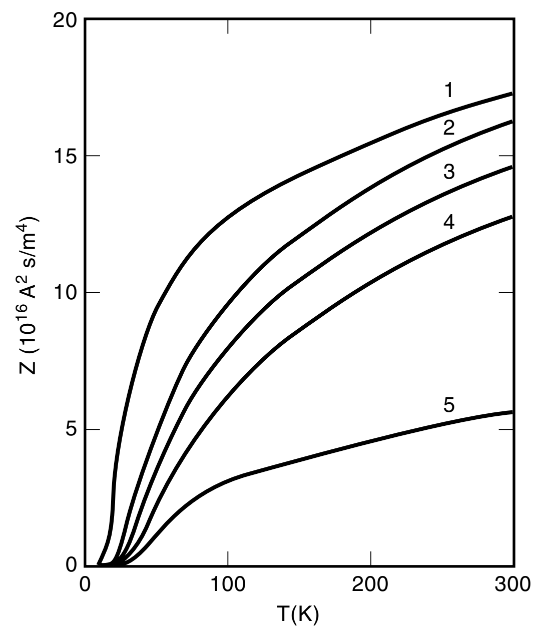

Figure 21. $Z(T_f)$ functions: (1) Silver (99.99%); (2) Copper (RRR 200); (3) Copper (RRR 100); (4) Copper (RRR 50); (5) Aluminum (99.99%) (30).

approximated as a volumetric ratio. The maximum allowable current density in the substrate is then

$$j_0 = \sqrt{\left(\frac{1+a}{a}\right)\frac{V_D I_0 Z(T_D, T_F)}{E_M}} \tag{9}$$

where V_D is the dump voltage (V), I_0 is the operating current (A), and E_m is the stored energy (J).

Iwasa's a-factor can be quickly estimated with a curve of volumetric specific enthalpies and the volumetric ratios of the different constituent materials in a design. The specific enthalpies of copper, aluminum, iron, nickel, niobium, titanium, tin, teflon, helium at 130 kg/m^3 and helium at 150 kg/m^3 are plotted from 4.5 K to 300 K in Fig. 20.

Copper and nickel are the two best materials above a maximum temperature of 100 K to 120 K. However, there is no more than a factor of two difference between the best and the worst metals. Copper is about 60% better than aluminum; but since aluminum is three times lighter than copper, it is twice as good as copper, if energy/mass is a more important consideration than energy/volume. Copper is clearly also the best material from an adiabatic J^2t criterion. Therefore, if the design is limited by the hot spot temperature in a given volume, copper is the material of choice.

The curves of $Z(T_f)$ versus T (K) in Fig. 21 appear in Iwasa's casebook (30).

While high-purity silver has the best $Z(T_F)$, far-less expensive oxygen-free coppers are nearly as good. Copper is two–three times as good as high purity aluminum. The $Z(T_F)$ versus T_F(K) curves in Fig. 22 were calculated specifically for a tradeoff between copper and stronger, less high purity aluminums. The curves show that copper is 20 to 25 times better than aluminum alloys. The implication is that the cross-sectional area of copper needed for protection in a design where the available enthalpy is dominated by the stabilizer would be four to five times less than that of aluminum. In a design in which other components, such as superconductor, helium, or other structures were important, the superiority of copper would be reduced. Magnetoresistivity would also reduce the quantitative superiority of copper. In magnetic energy storage designs, the main factor that improves the relative position of aluminum is that an aluminum such as 2219 can also be used as a structural material. In a design that requires a structural cross-section that is several times larger than the cross-

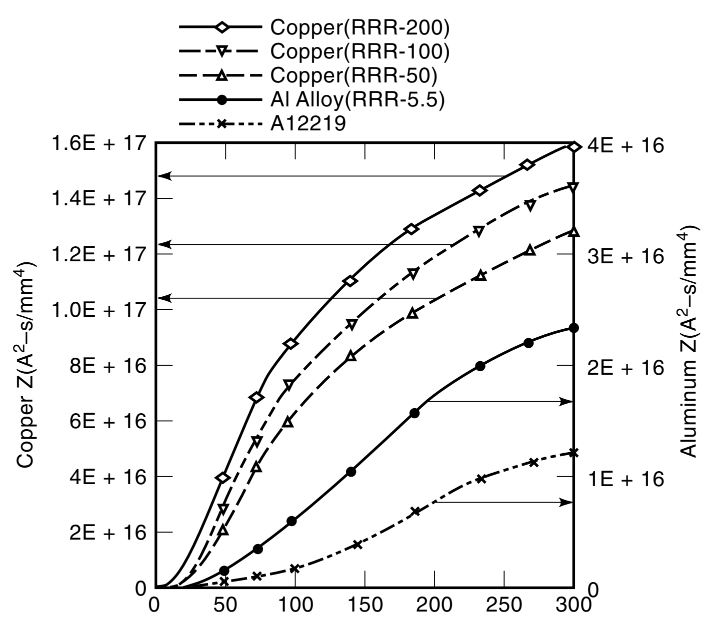

Figure 22. $Z(T_f)$ functions: (1) Copper (RRR = 200), (2) Copper (RRR = 100), (3) Copper (RRR = 50), (4) Aluminum alloy (RRR = 5.5), (5) Aluminum alloy 2219.

Table 3. $Z(T_f)$ Functions for Copper and Aluminum

Temperature	Copper, RRR = 200	Copper, RRR = 100	Copper, RRR = 50	Al Alloy (RRR = 5.5)	Al2219-T85
4	0	0	0	0	0
10	3.173×10^{14}	1.597×10^{14}	7.953×10^{13}	2.280×10^{12}	5.688×10^{11}
20	4.776×10^{15}	2.481×10^{15}	1.256×10^{15}	2.584×10^{13}	6.422×10^{12}
50	3.847×10^{16}	2.798×10^{16}	2.005×10^{16}	9.466×10^{14}	2.517×10^{14}
75	6.757×10^{16}	5.457×10^{16}	4.283×10^{16}	2.898×10^{15}	8.521×10^{14}
100	8.633×10^{16}	7.274×10^{16}	5.990×10^{16}	5.538×10^{15}	1.827×10^{15}
145	1.097×10^{17}	9.567×10^{16}	8.206×10^{16}	1.050×10^{16}	4.055×10^{15}
190	1.285×10^{17}	1.142×10^{17}	9.793×10^{16}	1.504×10^{16}	6.451×10^{15}
240	1.410×10^{17}	1.268×10^{17}	1.116×10^{17}	1.941×10^{16}	9.016×10^{15}
273	1.505×10^{17}	1.360×10^{17}	1.192×10^{17}	2.195×10^{16}	1.062×10^{16}
300	1.561×10^{17}	1.416×10^{17}	1.247×10^{17}	2.386×10^{16}	1.186×10^{16}

section needed for protection, the volumetric advantage of copper would disappear.

The values of $Z(T_f)$ from Fig. 22 are listed in Table 3.

QUENCH PROPAGATION

Adiabatic (Potted) Magnets

Adiabatically cooled magnets are selected for applications that are relatively small, and quasi-steady state, since they are incapable of absorbing large amounts of local energy. They are particularly suited to applications where there can't be any cryogenic fluid within the magnet and where small, compact winding packs are required. Iwasa has argued convincingly (31) that most high-temperature superconductor (HTS) magnets are also likely to be adiabatically cooled, because the local energy absorption is improved by orders of magnitude at higher temperatures.

Adiabatically cooled magnets may be protected either by internal or external energy dumps. If the simplifying assumption is made that the thermal conductivity and heat capacity of all materials is temperature independent, the longitudinal quench propagation velocity is expressed by the balance of constant local heating density and thermal diffusion through the winding pack as (30)

$$v_{\text{propagation}} = J\sqrt{\frac{\rho_n k_n}{C_n C_s\left(\dfrac{T_{cs}+T_c}{2}T_{op}\right)}} \tag{10}$$

where $v_{\text{propagation}}$ is the longitudinal quench propagation velocity in the winding direction (m/s), J is the current density in the composite wire (A/m^2), ρ_n is the electrical resistivity of the composite wire (W-m), k_n is the thermal conductivity of the normal wire (W/m-K), C_n and C_s are the heat capacities of the wire in its normal and superconducting states respectively (J/kg-K), and T_{op}, T_c, and T_{cs} are the operating and superconductor transition temperatures, respectively (K) (32). Again, because the heat capacity of all materials rises much more quickly with temperature than resistivity does, the quench propagation velocity of HTS quenches should be much lower than that of LTS quenches and the coils will be harder to protect.

Pool-Boiling Magnets

Pressure Rise. The quench pressure rise during the quench of a pool-boiling magnet involves a design tradeoff. The maximum pressure can most easily be controlled by the setting of external pressure relief valves or rupture disks (33). The additional pressure in the magnet due to pressure drops in the vent lines and the disks or valves can be solved by the time-dependent model of Krause and Christensen (34), assuming frictional, adiabatic (Fanno) flow in the vent lines. An alternative, recommended by Powell (35) is repressurization with warm helium gas. The motive for maintaining a high pressure, discussed in the section on electrical integrity, is that it will improve the dielectric strength of warm helium. The disadvantage is that it will increase the required thickness of the liquid helium cryostat, the pulsed eddy currents in the thicker cryostat, and the conduction losses through the cold mass supports.

Quench Propagation. Under normal conditions of cooling by a pool of liquid helium, the propagation velocity should obey the proportionality (36):

$$v_p = a(j_0 - j_r) \tag{11}$$

where j_r is the current density at which the conductor would recover (A/m^2), and j_0 is the operating current density (A/m^2). If the quench condition causes local dry out, then the propagation velocity is simply (37)

$$v_p = aj_0 \tag{12}$$

CICC Magnets

Quench propagation in CICC conductors is usually treated as a one-dimensional problem, quench propagating from an interior normal zone toward the inlet and outlet of a hydraulic channel. Bottura has written a general three-dimensional numerical solution for quench propagation (38), which, to the best of our knowledge, is also the only commercially available general quench propagation solution for any coil topology. However, since three-dimensional effects have only a second-order effect on the key design parameters of temperature, pressure, and expulsion velocity, one-dimensional solutions are still used.

Whole Coil Normal. In the extreme case of the whole coil going normal at once, quench propagation isn't an issue. This may help to place conservative upper bounds on peak pressure and expulsion velocity for design purposes. Note that simultaneous quench of a whole coil is not a worst case for hot spot temperature. If the coil is designed for internal energy absorption, it is a best case, because the peak/average energy absorption in the coil would be 1.0. If it is designed for external energy absorption, it may be a worst case for the refrigerator by absorbing energy at cryogenic temperature, instead of externally at room temperature; but in terms of the hot spot defined by the local J^2t, it is not a worst case, because the nonlinear dump time can only be accelerated by adding a larger internal coil resistance to the external resistance. Dresner (39) derived a simple expression for the pressure rise, if an entire hydraulic channel goes normal at once. This case would correspond to practical designs in which a resistive heater was used to ensure uniform internal energy absorption or to an external, uniform energy source being applied to a layer with nearly uniform temperature and field:

$$P_{\max} = 0.65\left(\frac{Q^2(L_{\text{coil}}/2)^3 f}{D_h}\right)^{0.36} \tag{13}$$

where Q is the volumetric heating of the helium (W/m^3), l is the half-length of the channel (m), and f is friction factor, and D_h is the hydraulic diameter (m). A cable-in-conduit has approximately three times the friction factor of a smooth tube with the same Reynold's number. For a quench pressure wave, Dresner adopts an approximate value of $f = 0.013$. When the pressure rise is not much greater than the initial pressure P_0 (Pa), the more exact formulation is

$$P_{\max} = 0.65\left(\frac{Q^2(L_{\text{coil}}/2)^3 f}{D_h}\right)^{0.36}\left(1 - \frac{p_0}{p_{\max}}\right)^{-0.36} \tag{14}$$

The same assumptions also predict (40) a helium expulsion velocity of

$$v_{\text{expulsion}} \simeq 0.952\left(\frac{Q\beta c_0}{\rho C_p}\right)^{2/3}\left(\frac{D_h t}{f}\right)^{1/3} \tag{15}$$

where Q is the volumetric heating of the helium (W/m^3), β is the constant pressure thermal expansion coefficient c_o is the isentropic sound speed (m/s), ρ is the helium density (kg/m^3), C_p is the helium specific heat at constant pressure (J/kg-K), D_h is the hydraulic diameter (m), f is friction factor, and t is the time since quench initiation (s). This solution is valid only for the beginning of a quench, since it assumes constant helium properties and neglects inertia and frictional heating.

Time-Dependent Normal Zone. Quench propagation scaling for long coils and uniform helium properties were first derived by Dresner (40). Dresner's scaling laws remain valid for describing the early stages of quench in a long hydraulic channel. However, the engineering limits of CICC coils are usually defined by the hot spot temperature, peak pressure, and peak helium expulsion flow toward the end of a quench. By this time, the material properties have changed significantly and heat absorption is dominated by the cable-and-conduit metal, rather than the helium. In this regime, the scaling of quench behavior is more complicated than that described by Dresner and the Shajii/Freidberg theory described next should be used.

Dresner's time-dependent equation for the pressure rise is

$$p - p_0 = C\rho c\left[\frac{4fZ}{D}\right]^{3/2}\left(\frac{D}{4fct}\right) \tag{16}$$

where C is a function of quench zone acceleration O(1), p_0 is the initial pressure (Pa), ρ is the helium density (kg/m^3), c is the velocity of sound in helium (m/s), f is the friction factor, Z is the length of the hot helium piston (m), D is the hydraulic diameter (m), and t is the quench time (s). In order to calculate the equivalent piston size, Wachi (41) makes the substitution:

$$CZ^{3/2} = 0.95t^{2.01} \tag{17}$$

Dresner's equation implies that the quench zone Z is

$$Z = \left[\frac{3(\gamma-1)}{2C(3+4\gamma)}\right]^{2/3}\left(\frac{Q^2Dt^4}{\rho^2c^2f}\right)^{1/3} \tag{18}$$

Similarly, Dresner solves for central pressure as function of time as

$$p = \frac{3(\gamma-1)}{3+4\gamma}Qt,\ p \gg p_0 \tag{19}$$

For helium, $\gamma = 5/3$, and if $C = 0.83$ for helium, as proposed by Dresner, these equations reduce to

$$Z = 0.25\sqrt[3]{\frac{Q^2Dt^4}{\rho^2c^2f}} \tag{20}$$

and:

$$p = 0.207Qt,\ p \gg p_0 \tag{21}$$

Shajii and Freidberg (42) rewrite the time dependences of Dresner's quench propagation equations for temperature, pressure, and quench propagation velocity as

$$T_{\text{Dresner}}(t) = \frac{0.10}{R\rho_0 L_{IQZ}}\left(\frac{4d_h}{f\rho_0^2c_0^2}\right)^{1/3}(\eta_0 J^2)^{5/3}t^{7/3} \tag{22}$$

where η_o is the resistivity of copper (Ω-m).

$$p_{\text{Dresner}} = 0.21\eta_0 J^2 t \tag{23}$$

and

$$V_{q\text{Dresner}} \equiv \frac{5}{4}\dot{X}_q = 0.42\left(\frac{4d_h}{f\rho_0^2c_0^2}\right)^{1/3}(\eta_0 J^2)^{2/3}t^{1/3} \tag{24}$$

Shajii Quench Theory. The Dresner equations were shown by Shajii and Freidberg to apply only in the operating space of short times, low conductor temperatures (<25 K), and long initial quench zones (43). Since this operating regime almost never includes the regimes of greatest interest for design (hot-spot temperature, peak pressure, peak expulsion velocity), it was necessary to develop solutions for other, more relevant regimes. Shajii and Freidberg derived analytic expressions for temperature, pressure, and quench zone propagation velocity for five other regimes, identified as the (1) short coil, low Δp, (2) short coil, high Δp, (3) long coil, low Δp, (4) long coil, high Δp, and (5) thermal hydraulic quenchback (THQB) regimes. In a short coil, the coil length is much shorter than the diffusion length of the quench zone, so that quench propagation is affected by end conditions. In a long coil, the mass of the coil channel is constant and propagation is unaffected by the ends. In the low Δp regime, the pressure rise due to the quench is $\ll p_0$, while it is $\gg p_0$ in the high Δp regime. An actual quench may have a trajectory in quench regime space that traverses two or more of these regimes. We use the nomenclature long coil and short coil here, because the usage has become accepted. However, it should be clarified that we are always discussing the length of a hydraulic channel, which is typically an order of magnitude shorter than a coil length. In all four of the constant mass quench zone solutions, Shajii derived scalings for the temperature and pressure, valid in the high-temperature (>20 K) regimes that are of interest as coil allowables. Assuming that the heat transfer coefficient h (W/m^2-K) is large:

$$\Delta T(t) = \frac{A_w \rho_w C_w}{2hP_w} \alpha(\bar{T}) J^2 \left(1 - e^{-t/\tau_w}\right) \tag{25}$$

where $\overline{T}$ is the average of the cable and conduit temperatures (K), and τ_w is a characteristic time constant for heat exchange between the cable and conduit (s):

$$\frac{1}{\tau_w} = hP_{\text{wall}} \left(\frac{1}{A_{\text{cable}} \rho_{\text{cable}} C_{\text{cable}}} + \frac{1}{A_{\text{wall}} \rho_{\text{wall}} C_{\text{wall}}} \right) \tag{26}$$

where h is the wall heat transfer coefficient (W/m^2-K), P_{wall} is the conduit wetted perimeter (m), A_{cable} and A_{wall} are the cable and wall cross-section areas (m^2), ρ_{cable} and ρ_{wall} are the mass densities of the cable and wall (kg/m^3), and C_{cable} and C_{wall} are the specific heats of the cable and wall (J/kg-K), respectively.

Short Coil Solutions. The criterion for a short coil solution is that the length of the coil is longer than the length of the quench zone, but less than the thermal diffusion length of the quench:

$$L < \sqrt{\frac{24 d_h c_0^2 t_m}{f V_q}} \tag{27}$$

where c_0 is the initial sound speed (m/s), d_h is the hydraulic diameter (m), V_q is the quench front velocity (m/s), and t_m is the time needed to reach the maximum allowable temperature $t_m \simeq T_{\max}/\alpha_0 J^2$.

Short Coil, High Pressure. A short coil quench will be in the high-pressure rise regime ($\Delta p > p_0$) when

$$\frac{\Delta p}{p_0} \simeq \frac{R \rho_0 \alpha_0 J^2 L_{IQZ}}{2 p_0 V_q} > 1 \tag{28}$$

where R is the universal gas constant (=8314.3 J/kg-mole-K, He = 4.003 kg/mole), ρ_0 is the background helium mass density (kg/m^3), J is the current density in the stabilizer (A/m^2), L_{IQZ} is the initial length of the quench zone (m), p_0 is the background helium pressure (Pa), d_h is the hydraulic diameter (m), f is the friction factor, assumed to be a constant in the range of 0.06–0.08, and α_0 is a diffusion constant of the conduit material (typically 5–7 $\times$ 10^{-6} m^4-K/A^{2}s), defined as

$$\alpha_0 \cong \min_T \left[\frac{A_{cu} \eta_c(T)}{A_c \rho_c C_c(T) + A_w \rho_w C_w(T)} \right] \tag{29}$$

where η_c is the thermal resistivity (W/m-K).

For a short coil in the high-pressure regime, the asymptotic quench velocity, once quench has been well initiated, is

$$V_q = \sqrt[3]{\frac{2dR}{fL_{\text{coil}}} L_{IQZ} \alpha_0 J^2} \tag{30}$$

where d is the hydraulic diameter (m) and f is the friction factor. The position of the forward quench front X_q (m), using the convention that all quenches are symmetrically centered about $x = 0$, is

$$X_q = \left[\left(\frac{L_{IQZ}}{2} \right)^{3/2} + (V_q t)^{3/2} \right]^{2/3} \tag{31}$$

Short Coil, Low Pressure. A short coil quench will be in the low-pressure rise regime ($\Delta p < p_0$) when

$$\frac{\Delta p}{p_0} \simeq \left(\frac{f \rho_0 L_{\text{coil}}}{4 d p_0} \right) V_q^2 < 1 \tag{32}$$

For a short coil in the low-pressure regime, the quench velocity is

$$V_q = \frac{R \rho_0 \alpha_0 J^2 L_{IQZ}}{2 p_0} \tag{33}$$

The short coil limit also provides a simple analytical expression for the density outside the normal zone as a function of length and time:

$$\rho(x,t) = \rho_0 + \left(\frac{\rho_0 f V_q^2}{2 d_h c_0^2} \right) \left(\frac{L_{\text{coil}}}{2} - x \right) \tag{34}$$

where ρ_0 is the initial density (kg/m^3). The density decreases linearly with x, while the velocity outside the normal zone is a constant versus both space and time.

Long Coil Solutions

Long Coil, High Pressure. The long coil solution is defined by the two criteria that the coil length is much greater than the length between diffusion edges $(L/2)^2 \gg X_D^2(t_m)$, and that the length of the quench zone is much less than the length between diffusion edges $[X_q^2 \ll X_D^2(t_m)]$. The criterion for the long coil solution can then be stated as

$$L_{\text{coil}}^2 \gg \frac{24 d_h c_0^2 t_m}{f V_q} \gg 4 V_q^2 t_m^2 \tag{35}$$

The long coil quench is in the high-pressure rise regime ($\Delta p > p_0$) when

$$\frac{\Delta p}{p_0} \approx \frac{R \rho_0 \alpha_0 J^2 L_{IQZ}}{2 p_0 V_q(t_m)} > 1 \tag{36}$$

The position of the forward quench front in the high-pressure regime is

$$X_q = \left[(L_{IQZ}/2)^{5/3} + (V_q t)^{5/3}\right]^{3/5} \tag{37}$$

where V_q is the asymptotic quench propagation velocity (m/s):

$$V_q = 0.613\left(\frac{2d_h}{f}\right)^{1/5}\left(\frac{RL_{IQZ}\alpha_0 J^2}{c_0}\right)^{2/5}\frac{1}{t^{1/5}} \tag{38}$$

(The multiplier of 0.613 differs from the two published values of 0.766 by a factor of 5/4, removing an ambiguity in interpreting the Shajii equations self-consistently.) The helium velocity (m/s) in the region outside the quench zone is

$$v(x,t) = \frac{0.8V_q t}{t + \lambda_1^2 (x - L_{IQZ}/2)^2} \tag{39}$$

where $\lambda_1^2 = \rho_0\,0.8V_q/3\nu_0^2$. The density profile for the density ρ in the outer region (kg/m^3) is given by

$$\begin{aligned}\rho(x,t) &= \rho_0 + \frac{9\nu_0^2}{2K^{3/2}}\left(\cot^{-1}\frac{\xi}{\sqrt{K}}\frac{\sqrt{K}\xi}{K+\xi^2}\right)\\ &\approx 3\nu_0^2\frac{\lambda_2^3 t^2}{\left[t^{3/4} + \lambda_2^{3/2}(x - L_{IQZ})^{3/2}\right]^2}\end{aligned} \tag{40}$$

where $\lambda_2(t) = (3\pi/4)^{1/3}\lambda_1$ and ν_0 is

$$\nu_0 = \sqrt{\frac{2d_h\rho_0 c_0^2}{f}} \tag{41}$$

Equation (11) implies that the expulsion velocity is given by

$$v(x = L_{\text{coil}}/2, t) \simeq \frac{24 d_h c_0^2}{f L_{\text{coil}}^2} t \tag{42}$$

This is the same expulsion velocity as that predicted by Dresner. However, with the exception of the expulsion velocity, Dresner's solutions for temperature, pressure, and quench velocity in Eqs. (16–18) have functional dependencies that are significantly different from Shajii's, even in the long-coil case.

Long Coil, Low Δp Regime. In the small Δp regime, the pressure rise remains small in comparison with the initial pressure ($\Delta p \ll p_0$), corresponding to a weak quench in which the helium coolant removes most of the heat generated by a quench. In the small Δp regime, the length of the quench zone is

$$X_q \approx \frac{R\rho_0 L_{IQZ}(\bar{T} + \Delta T - \bar{T}_{t=0+})}{2p_0} + \frac{L_{IQZ}}{2} \tag{43}$$

where $\overline{T} = (T_{\text{cable}} + T_{\text{wall}})/2$ and $\Delta T = (T_{\text{cable}} - T_{\text{wall}})/2$. $t = 0+$ means the time immediately after the initial quench zone has been established, assuming sudden energy deposition.

The quench velocity is then

$$V_q \approx \frac{R\rho_0\alpha_0 J^2 L_{IQZ}}{2p_0} \tag{44}$$

The low Δp itself is given by

$$\Delta p(t) = 9\nu_0^2 c_0^2 t^2 \int_{X_q}^{L_{\text{coil}}/2} \frac{dx}{\left[(x - L_{IQZ}/2)^2 + X_D^2\right]^2} \tag{45}$$

where the leading edge of the diffusion front X_D (m) is

$$X_D^2 = \frac{3\nu_0^2}{\rho_0}\frac{t}{V_q} \tag{46}$$

For the combined short coil plus small Δp case, the solution for Δp reduces to Eq. (23). For the combined long coil plus small Δp case, the solution for Δp reduces to

$$\Delta p(t) = 1.36\left(\frac{f}{2d_h}\right)^{1/2}\rho_0 c_0 t^{1/2} V_q^{3/2} \tag{47}$$

Universal Scaling Regimes. Shajii recast the preceding criteria into a universal form that predicts the boundaries between the four quench regimes. Two dimensionless variables x and y are defined and all quench regimes are shown as filling four corners of x–y space. First a dimensionless variable λ and a dimensional variable $L_0J_0^{4/3}$ (A$^{4/3}$/m$^{5/3}$) are defined:

$$\lambda = 1.7\left(\frac{\rho_0 R T_{\max}}{p_0}\right)\left(\frac{c_0^2\rho_0}{p_0}\right) \tag{48}$$

where ρ_0, c_0, and p_0 are the density (kg/m^3), sound speed (m/s), and pressure (Pa) of the background helium. R is the universal gas constant (8314.3 J/kg-mole-K), and $T_{\max}(x,t)$ is the maximum temperature of the quench zone (K).

$$L_0 J_0^{4/3} = \frac{2.6}{R}\sqrt[3]{\frac{p_0^5 d}{f\alpha_0^2 c_0^2 \rho_0^5 T_{max}}} \tag{49}$$

λ and $L_0J_0^{4/3}$ tend to be relatively constant over a wide range of time and space for a given design. In order to distinguish better between the widely different quench regimes, these variables are reordered by being normalized to the strongly varying J (A/m^2) and L_q (m):

$$x = \frac{\lambda L_q}{L} \tag{50}$$

$$y = \frac{L_q J^{4/3}}{L_0 J_0^{4/3}} \tag{51}$$

This now allows the criteria for entry into each of the four quench regimes to be written in the following simple universal form:

Quench Regime	Pressure Condition	Length Condition
Long coil, high pressure	$y > 1$	$y > x^{5/6}$
Short coil, high pressure	$y > 1.2x^{1/3}$	$y < 1.1x^{5/6}$
Long coil, low pressure	$y < 0.8$	$y > x^{2/3}$
Short coil, low pressure	$y < 1.2x^{1/3}$	$y < x^{2/3}$

The four universal scaling regimes are shown in Fig. 23.

Thermal-Hydraulic Quenchback. The misnomer thermal-hydraulic quenchback (THQB), which is certainly thermohy-

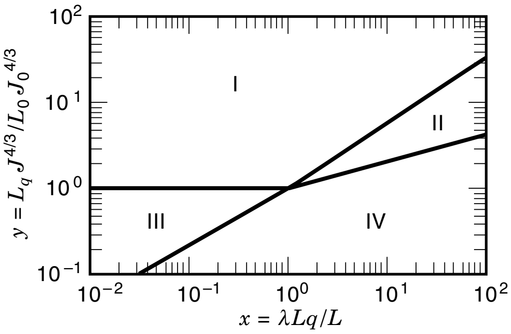

Figure 23. Boundaries in x–y space defining the four quench regimes: (I) long coil-high pressure rise, (II) short coil-high pressure rise, (III) long coil-low pressure rise, and (IV) short coil-low pressure rise [Shajii, 1995 (44)].

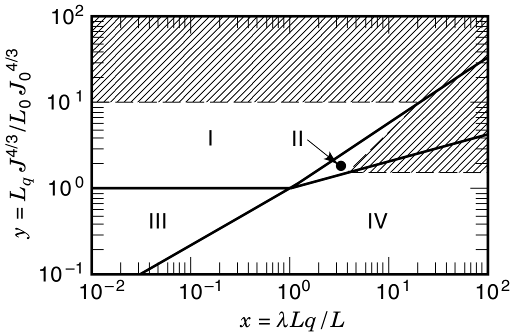

Figure 24. Scaling diagram showing dimensionless quench regime boundaries for $M = 4$.

draulic, but has nothing to do with quenching backwards, has become sufficiently popular as a term that we won't try to rename it Joule-Thomson quench propagation. It refers to a condition in which compression heating of helium in front of a quench zone leads to rapid propagation of quench in which the thermal/quench wave travels much faster than the mass flow of helium expulsion in front of the quench zone. A key dimensionless parameter in predicting whether there can be a rapid onset of THQB, again introduced by Shajii (44), is the safety margin between current sharing and background temperature M:

$$M = \left[\frac{C_h(T_0)}{C_\beta(T_0)}\right]\left(\frac{\rho_0 c_0^2}{p_0}\right)\left(\frac{T_{cs} - T_0}{T_0}\right) \tag{52}$$

Typically $M \sim 2$ to 5 for practical coils. Another parameter β is needed to account for the finite ratio of frictional to compressive heating in the THQB regime:

$$\beta = \frac{C_\beta(T_0)\rho_0 T_0}{p_0} \tag{53}$$

β is typically of order unity.

THQB cannot exist long in the low pressure rise regime. In the long-coil, high pressure rise regime, the temperature just ahead of the quench front can be written as:

$$T_f(t) \approx T_0 + \frac{1}{2}\left[\frac{C_\beta(T_0)}{C_h(T_0)}\right]\frac{RT_0\alpha_0 J^2 L_q}{c_0^2 V_q(t)} \tag{54}$$

This expression includes the effect of compression heating, but not of frictional heating.

The condition for THQB to occur before $T = T_{\max}$ is

$$y > M^{5/3} \tag{55}$$

For the short coil-low pressure rise regime, the condition for THQB to occur before $T = T_{\max}$ is

$$y > \beta^{1/3} M^{1/3} \tag{56}$$

The temperature ahead of the quench front is then

$$T_f(t) = T_0 + \left[\frac{fV_q^3}{2dC_h(T_0)}\right]t \tag{57}$$

In the short coil-high pressure rise regime, frictional heating must again be included, and the condition for THQB to occur before $T = T_{\max}$ is

$$y > \frac{x^{1/3}}{2}\left\{1 + \left[1 + 4(x - M)\right]^{1/2}\right\} \tag{58}$$

where β and other numerical coefficients have been set to unity.

The intersection of the THQB regime with the four universal regimes for a typical case of $M = 4$ is shown in Fig. 24.

Unique THQB shaded regions can be calculated for every value of M.

ELECTRICAL INTEGRITY

A superconductor has no voltage in the quiescent state and may have a very low voltage, during startup and shutdown, depending on the application. In the majority of applications, the superconducting magnet will experience its highest design voltages during a quench dump. It is also during a quench dump that the helium temperature will be highest, helium density in electrical isolators may be decreased by pressure relief valves, and liquid will be boiled into vapor. All of these effects can simultaneously increase electrical fields, while decreasing the ability of helium or insulation voids to withstand the electrical fields. Arcs have developed during operation of real superconducting magnets and are a known cause of failure and life limitation.

Breakdown in Helium

In a pool-boiling magnet, helium is the primary insulation. Design against helium breakdown must include the winding-pack, joints, supports, vapor-cooled leads, feedthroughs, and room-temperature isolators. In CICC magnets, the problem is restricted to specially designed helium isolators, providing the electrical isolation between the magnets and its grounded helium headers. However, CICC magnets have the special problem of protecting feedthroughs and leads against low-

Table 4. Paschen Minimum Gaps and Gaps at 20 kV, According to Olivier Equation

Pressure (atm)	Temperature (K)	Density (kg/m^3)	Gap at Paschen Minimum (mm)	Gap at 20 kV (mm)
1.0	4.229	127, liquid	7.9×10^{-5}	0.133
		15.2, vapor	6.6×10^{-4}	1.17
3.0	5.0	117	8.5×10^{-5}	0.144
3.0	150	0.973	0.011	20.0
10^{-4}	5.0	10^{-3}	10	20,000
1.0	273	0.178	0.056	112

density helium breakdown, in the event of a helium leak. The primary motivation for dry superconducting magnets is to avoid this problem altogether, while accepting a low energy margin against disturbances.

The dielectric strength of liquid helium is comparable to that of air at standard temperature and pressure. Unfortunately, since breakdown accompanies heating due to a normal event and rapidly heats local helium, the actual breakdown strength of liquid helium in a magnet is hard to interpret. It is conservative and probably correct to always consider gaseous helium to be the insulator in a pool boiling magnet.

The breakdown strength of gaseous helium at ambient temperature is only a small fraction of that of air because the electrons can gather kinetic energy from electrical field drift up to the ionization level in the noble gas helium. Paschen's law should hold for gaseous helium at any temperature. At all density-gap products that are well above the minimum of the Paschen curve, the dielectric strength of helium is at least a factor of 10 worse than that of nitrogen or air.

In the high-pressure regime of the Paschen curve, Olivier showed that a direct exponential correlation can predict the voltage breakdown for a broad range of gases, including helium, in a uniform field over a broad range of gap lengths and pressures (45). At any temperature, the breakdown voltage between spherical electrodes is

$$V_{\text{breakdown}} = K\rho^{\alpha} d^{\beta} \tag{59}$$

where K is a constant, ρ is the mass density of helium (moles/liter), d is the gap (mm), and α and β are the exponents. According to Olivier, for helium $\alpha = 0.878$, $\beta = 0.901$, and $K = 4310$. Thus, for helium at STP, where one mole = 22.4 L and the density of helium is 4 g/22.4 L = 0.178 kg/m^3, the general equation for voltage breakdown with the gap d in m, the breakdown voltage V in volts, and the density ρ in kg/m^3 would be

$$V_{\text{breakdown}} = 645,375\rho^{0.878} d^{0.901} \tag{60}$$

The density-gap product that produces the minimum of 160 V in helium is 10^{-5} kg/m^3-m. The gaps at the Paschen minimum and the gaps predicted for breakdown at 20 kV by the Olivier equation are shown in Table 4.

A Paschen curve through several sets of experimental data is shown in Fig. 25.

At cryogenic temperatures the breakdown strength of helium in uniform field allows for a straightforward design in pool boiling magnets, where it can be guaranteed that breakdown will occur in the high density-distance regime. Figures 26 and 27 (46) show that with minimum breakdown fields on the order of 10 MV/m, each millimeter of gap should be adequate to protect against 10 kV.

However, breakdown in helium is highly sensitive to electric field nonuniformities and to field polarity. Figure 28 (47) depicts low temperature dc breakdown characteristics for he-

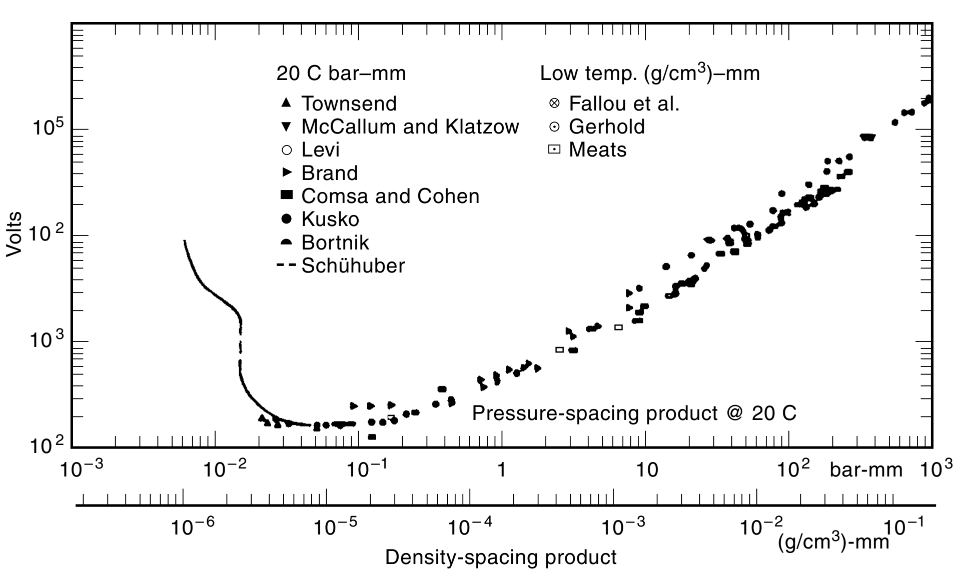

Figure 25. Paschen curve for helium.

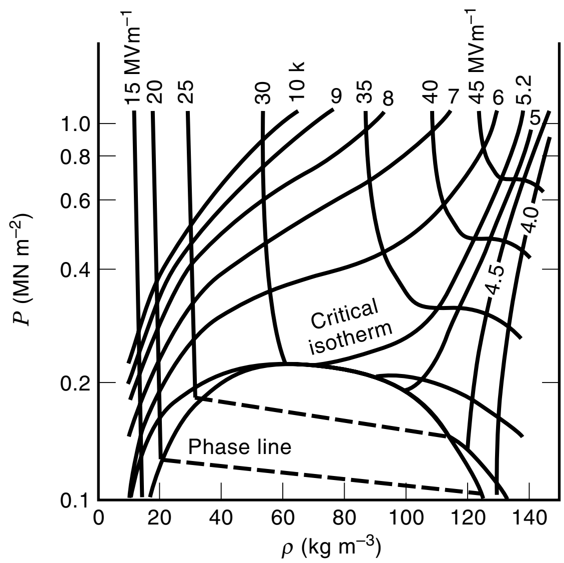

Figure 26. Depicts the breakdown strength of helium as a function of pressure and density, under uniform field conditions [Gerhold, 1979 (48)].

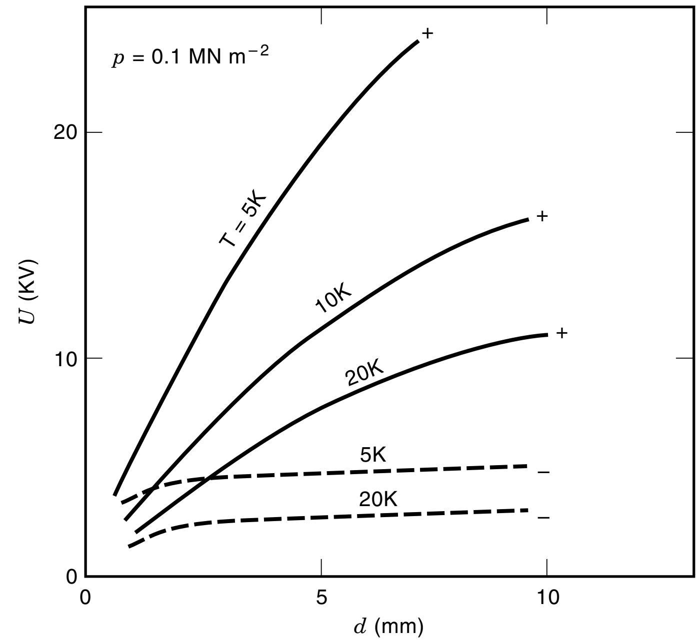

Figure 28. Helium nonuniform field breakdown voltages in low temperature helium gas at atmospheric pressure [Gerhold, 1979 (48)].

lium gas under nonuniform (point to plane) field conditions at atmospheric pressure (48).

The strong polarity dependence is evident in this figure, suggesting that the design of the electrode configuration to maintain a field as close to uniform as possible is particularly important, when feasible. The breakdown level is also a function of electrode surface material and conditions (49), conditioning, and electrode polarity (50).

A design approach proposed to avoid striking an arc across a helium gap is to use the dielectric strength of helium at the design temperature and atmospheric pressure for a sharp point at a 3 mm gap between the point and the plain (51). At 4 K, the breakdown strength of helium is 60 V/mil (2.36 kV/mm), at 10 K, the breakdown strength is 24 V/mil (944 V/mm), and at 100 K, the breakdown strength is 2.4 V/mil (94 V/mm).

Electric Field Concentrations

Solid insulations are seldom designed with electrical fields higher than 10–20% of their intrinsic dielectric strength. This is not merely an expression of extreme conservatism toward catastrophic punchthrough and arcing, but also reflects the reality of electrical field concentrations in practical designs. While many solid insulations have dielectric strengths >100 kV/mm, it has been shown that the presence of small voids in a solid will cause the inception of particle discharges in low temperature helium at electric fields of 10 kV/mm to 20 kV/mm (52). There is some evidence that the minimum breakdown voltage in a helium void may saturate at low density and that there is no left-hand side of the Paschen curve in voids. Measurements by Hiley and Dhariwal (53) appear to saturate at 4.5 kV/mm in polyethylene at zero density for a cavity depth of 0.2 mm (900 V). In epoxy resin, they appear to saturate at 1.2 kV/mm for a cavity depth of 0.2 mm (240 V).

Partial discharges in solid insulation voids are caused by high electric fields in the voids. These will not destroy the insulation, if they are infrequent, but can cause erosion of organic insulation in a pulsed application.

The electric field in a void tends to be higher than that of the solid insulation itself because the dielectric constant of solid insulations is always higher than that of free space. Further electric field multipliers are caused by shape factors in the void, where breakdown can be further enhanced by nonuniform electric field within the void itself. Analytic solutions are available for the electric field concentrations in planar, spherical, and cylindrical voids. For other shapes, numerical techniques are available to calculate the electric field concentrations for both 2-D and 3-D shapes. Engineering rules of thumb also exist for the most likely void shapes. Zahn (54) developed the following derivation of the electric field concentrations in spheres and cylinders.

Voids in Solid Insulation. The simplest model assumes that a void region exists within a uniform dielectric that has an essentially uniform electric field in the vicinity of the void.

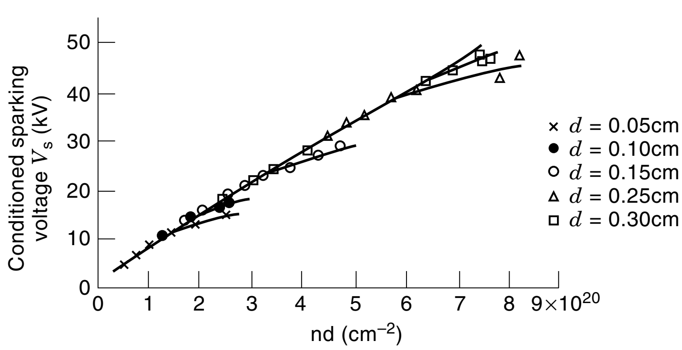

Figure 27. Depicts low temperature (<10 K) dc breakdown characteristics for helium gas under uniform field conditions [Meek, 1979 (47)].

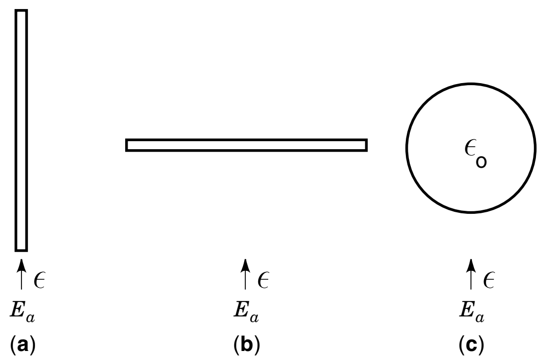

Figure 29. Three void orientations versus electric field in dielectric medium.

We consider three simple cases shown in Fig. 29 of uniform electric field incident on (1) a long, thin void, either planar or cylindrical, with the long axis in the direction of the electric field; (2) a long thin void, either planar or cylindrical, with the long axis perpendicular to the electric field; and (3) a spherical void. Cases (1) and (2) form easily at an interface between dissimilar materials, while case (3) can arise due to gassing. If the void region is air at ambient temperature and pressure, the electrical breakdown strength is $E_b \sim 3$ kV/mm. Fields above E_b will result in spark discharges. The maximum external electric field outside the void can then be calculated that would keep the voidage electric field below E_b.

Long Thin Void Along Electric Field. Because the tangential component of an electric field is continuous across an interface, the electric field

$$\overline{E}_v = \overline{E}_a \tag{61}$$

This result is valid for planar and cylindrical voids.

Long Thin Void Perpendicular to Electric Field

Planar Void. For highly insulating dielectrics with dielectric relaxation times ($\tau = \epsilon/\sigma$) much greater than the time scales of a quench, the normal component of the electric displacement field, $\overline{D} = \epsilon\overline{E}$ must be continuous across an interface. Thus

$$\epsilon\overline{E}_v = \epsilon\overline{E}_a \rightarrow \epsilon\overline{E}_v = \frac{\epsilon}{\epsilon_0}\overline{E}_a \tag{62}$$

The higher the dielectric permittivity of the insulation surrounding the void, the lower the applied electric field must be to keep $\overline{E}_v < E_b$.

Cylindrical Void. In the absence of any volume charge in a uniform permittivity dielectric, Laplace's equation can be solved in cylindrical coordinates for the electrical field inside and outside the cylindrical void:

$$\begin{aligned} \overline{E} &= 2\frac{\epsilon}{\epsilon + \epsilon_0}\overline{E_a}\dot{i}_x & 0 < r < R \\ \overline{E} &= E_a\left[1 + \frac{R^2}{r^2}\frac{(\epsilon_0 - \epsilon)}{(\epsilon_0 + \epsilon)}\cos\varphi\dot{i}_r \right. \\ &\quad \left. - \left(1 - \frac{R^2(\epsilon_0 - \epsilon)}{r^2(\epsilon_0 + \epsilon)}\sin\varphi\dot{i}_\varphi\right)\right] & r > R \end{aligned} \tag{63}$$

Table 5. Dielectric Constant ε

Material	Dielectric Constant ($\varepsilon_r/\varepsilon_0$)
Kapton polyimide film 120CI-1	3.5
Kapton polyimide film 135RCI	3.8
G10-CR	4.9–5.0
G11-CR1	5.1–5.2

The internal electric field is purely x directed, while the external electric field has the applied uniform electric field plus a line-dipole field. To avoid breakdown in the cylindrical void

$$2\frac{\epsilon}{\epsilon + \epsilon_0}E_a < E_b \tag{64}$$

Spherical Void. The general form of solution to Laplace's equation in spherical coordinates for a uniform z directed electric field is

$$\varphi = \left(Ar + \frac{B}{r^2}\right)\cos\theta \tag{65}$$

The total electric field inside and outside the cylindrical void is

$$\begin{aligned} \overline{E} &= \frac{3\epsilon}{2\epsilon + \epsilon_0}E_a\overline{i_z} & 0 < r < R \\ \overline{E} &= E_a\left[\left(1 + 2\frac{R^3}{r^3}\frac{(\epsilon_0 - \epsilon)}{(2\epsilon + \epsilon_0)}\right)\cos\theta\overline{i_r} \right. \\ &\quad \left. - \left(1 - \frac{R^3}{r^3}\frac{(\epsilon_0 - \epsilon)}{(2\epsilon + \epsilon_0)}\right)\sin\theta\overline{i_\theta}\right] & r > R \end{aligned} \tag{66}$$

The internal electric field is purely z directed, while the external electric field has the applied uniform electric field plus a point dipole field. To avoid breakdown in the spherical void:

$$\frac{3\epsilon}{2\epsilon + \epsilon_0}E_a < E_b \tag{67}$$

Dielectric constants of some widely-used solid insulations are listed in Table 5.

The electric field multipliers for other commonly found void shapes are listed in Table 6.

The multipliers for laps and voids in corners are typical values, based on numerical analysis.

A conservative way to look at the design rules for solid insulation would be to design so that partial discharges in the solid insulation were impossible, irrespective of the partial

Table 6. Electric Field Multipliers for $\varepsilon = 3$ Insulation System

Shape	Multiplier
Infinite plane or cylinder, parallel to field	1
Infinite plane, transverse to field	3
Infinite cylinder, transverse to field	1.5
Sphere	9/7 = 1.286
Cusp/crescent (debonding at a rounded corner)	1.6–1.7
Triangle (e.g., epoxy/kapton lapping)	1.6–1.8

pressure in the insulation voids. As an example, in a superconducting magnet, the worst gas and the most likely gas to have a partial pressure is helium, whose Paschen minimum is 160 V. Adopting 2 kV/mm as a typical allowable for glass-epoxy and a geometry/dielectric constant mismatch multiplier of 2, this design rule would then put the burden on the mechanical design to assure that the largest possible void in the solid insulation would be

$$d_{\text{max,allowable}} \leq \frac{V_{\text{Paschen min}}}{E_{\text{max,allowable}} R_{\text{mult}}} = \frac{160\,V}{2\dfrac{kV}{mm} x\, 2} = 0.040\,mm \tag{68}$$

For example, if a conduit with a slip-plane wrap bowed in 10 μm, this would be acceptable, since breakdown of helium would still be impossible.

Stray Coil Capacitance

The turn-turn and layer-layer voltages across a winding pack are not exactly equal, even in the absence of any resistance. The turns in a winding pack don't all link exactly the same amount of flux, particularly in multicoil systems. The peak-average ratios in coil systems we have investigated were in the range of 1.1–1.3 : 1. A more serious, but avoidable, problem comes from the possibility of overvoltages due to distributed capacity charging of the winding pack. There is a distributed capacitance between every turn of the winding pack and to ground, as illustrated by the circuit model, shown in Fig. 30. Mutual capacitance to nonadjacent turns is neglected.

The peak local electrical field is higher than what would be predicted considering only the coil resistance because of stray coil capacitance in the insulation. The voltage enhancement factor is a function of α:

$$\alpha = \sqrt{\frac{C_g}{C_s}} \tag{69}$$

where C_g is the shunt capacitance to ground and C_s is the series capacitance. For fast rise times and large values of α, half of the terminal voltage can appear between the first two turns of the coil. Measurements on the POLO coil (55) and analyses at Karfruke (KfK) and M.I.T. showed that large voltage enhancements could be avoided, if the voltage rise time were long enough. This is a tradeoff, since switch losses or counterpulse circuit size is proportional to the voltage rise

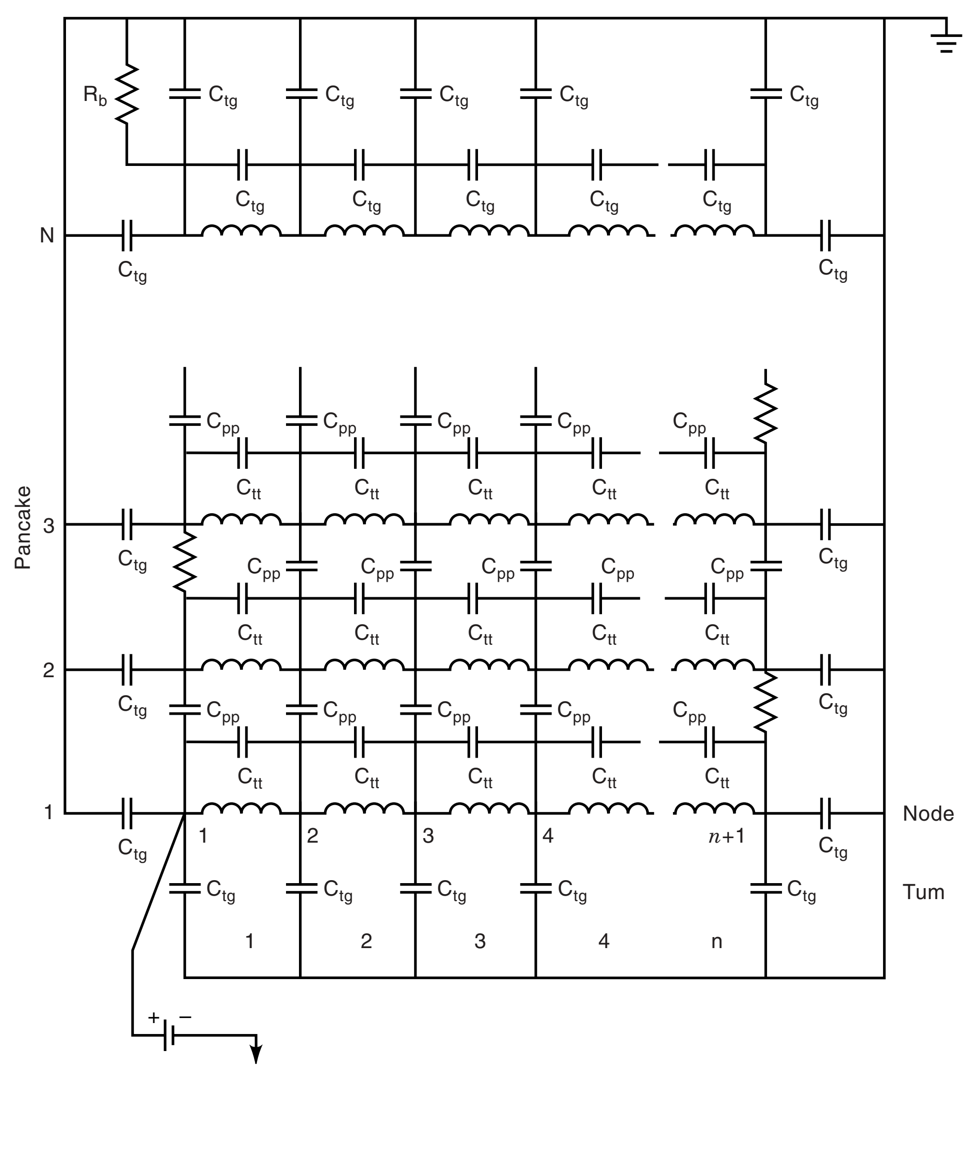

Figure 30. Distributed capacitance/inductance network model of a winding pack and ground insulation.

time. Optimization of the cost/performance trade can be done for a specific design, using commercial circuit codes. However, since the ringing time is primarily a function of conductor size only, analysis indicates that it is safe over a broad range to limit the voltage rise time to >100 μs, if the conductor is <5 cm square.

Tracking Along an Insulating Surface

Tracking is the leakage current due to the formation of a conducting path across the surface of an insulation. In most cases, the conduction results from degradation of an organic insulation. The conducting film is usually moisture from the atmosphere absorbed by some form of contamination, such as dust. Tracking does not depend upon Paschen breakdown and can occur at well below 100 V in air, while a gaseous discharge in air cannot exist below 380 V. Degradation of the insulation is caused by heat from tracking, which either carbonizes or volatilizes the insulation. This implies that insulations in helium or vacuum at liquid helium temperatures should be more immune to tracking than magnets in air, because of the absence of chemical reactions. Carbonization results in a permanent extension of the electrodes and usually takes the form of a dendritic growth; but erosion of the insulation also occurs.

Configurations for which tracking is particularly important are those where a high voltage conductor emerges from an insulated lead. Generally a conducting electrostatic shield or ground plane will surround the lead insulation, but will be terminated at some point, leaving a tracking path along the surface of the lead insulation from the end of the ground plane to the conductor itself. The electric field is enhanced at the end of the electrostatic shield in this configuration, and can lead to local ionization which effectively extends the ground electrode, due to space charge, and reduces the useful length of the tracking path, such that the discharge advances along the surface toward the lead, with eventual flashover. Figure 31 illustrates tracking at a high voltage lead termination.

Common practice is to utilize a stress cone (a specially shaped electrode) or a stress grading material or coating on the surface of the lead insulation just after the termination of the conducting electrostatic shield. The effect of the stress grading is to reduce the maximum field gradient based on the nonlinear voltage versus current characteristic of the stress grading material. Silicon carbide is a commonly used material for stress grading, and is available in tape and paint binders.

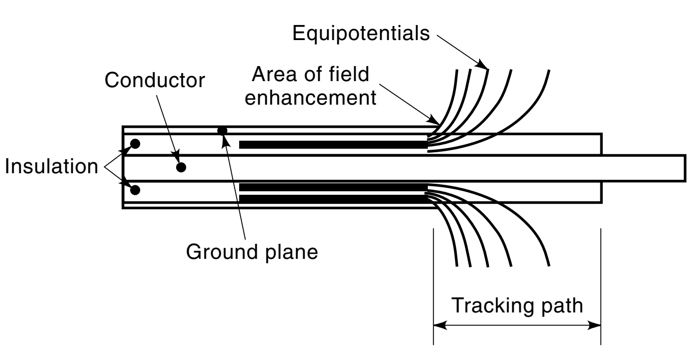

Figure 31. Tracking at high voltage lead termination.

Heat shrinkable stress grading tubing is also available, and is normally used in the termination of high voltage cables. This material could offer a solution to the problem of temporary stress grading during test, when the termination of high voltage leads is not in its final configuration.

Yet another technique is to cover the entire termination in an insulating jacket. The effect is to contain the areas of highest stress in a solid dielectric, and to increase the tracking path length that must be taken by a discharge which would directly connect the high voltage electrode with the ground electrode.

To the extent that the high voltage conductors can be fully insulated and enclosed by an electrostatic shield, the tracking problem in the near vacuum environment can be avoided. However, the high voltage conductors such as the main high current leads and any instrumentation (e.g., voltage tap) conductors must eventually emerge from the insulation.

The helium supply lines which must bridge the gap between the high voltage conductors and ground present another potential tracking path. Considering a configuration consisting of a metallic pipe emerging from the main conductor which delivers the coolant to an insulating tube, which in turn connects to a grounded metallic pipe associated with the manifold. Tracking on the outer surface of the insulating tube could be a problem, particularly in the cryostat vacuum environment which can be compromised by helium leaks. This problem can be solved by encapsulating the region of transition from high voltage, through the insulator, to ground, in a solid dielectric contained within an electrostatic shield. In this case the path which would otherwise be available for tracking, and the entire region subject to electric stress, can be fully contained in solid insulation, as illustrated in Fig. 32.

Experimental Basis for Tracking Allowables. Migliori, Schermer, and Henke (56) measured dielectric tracking fields in liquid helium for four gaps in a G-10 circuit board. The minimum tracking strength that they measured was 13.7 kV/mm at 0.48 mm. They reported that the cleanliness of the sample, that is, whether it was abraded with copper or wet-wound with metal inclusions, made little difference in the tracking strength. They also reported that the breakdown field declined as $d^{-0.25}$ and that the tracking strength was that of helium vapor, rather than that of liquid helium. This is a somewhat misleading conclusion, because the tracking strengths that they measured were similar to those measured earlier by Haarmon and Williamson (57) in liquid helium, and orders of magnitude superior to Haarmon and Williamson's measurements in gaseous helium. The earlier experiment reported nearly identical tracking breakdown fields for paper phenolic, polyethylene, nylon, and teflon. Their measurements of the tracking strength for series of five 60 kV, 500 ms, half sine-wave pulses with descending gap are shown in Table 7.

For design purposes, the relevant numbers are those for gaseous helium at 4 K and 293 K. Fortunately, the temperature sensitivity is rather small, varying only a factor of two at most over a temperature range of 75 : 1. A factor of four safety margin would imply that tracking should be limited to 100 V/mm (2.5 V/mil). Designs have been identified with tracking fields in the range of 60 V/mm to 200 V/mm.

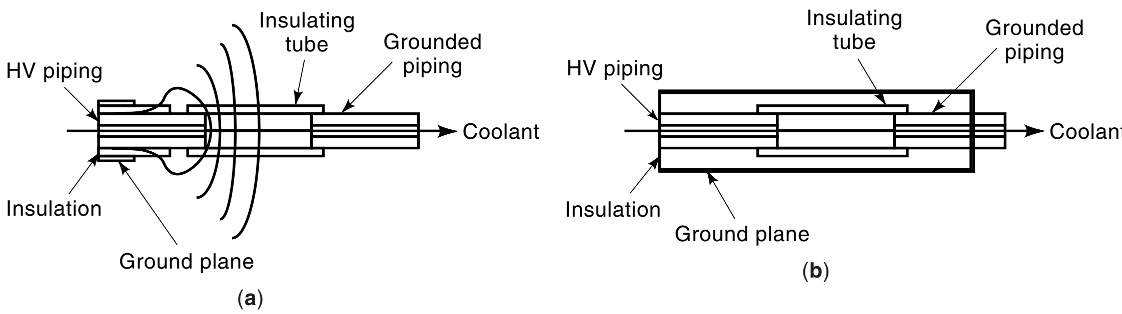

Figure 32. Avoidance of tracking with full-insulated coolant connections. (a) Tracking at coolant connection. (b) Fully insulated coolant connection.

Electrical Design Allowables

For design purposes, typical electrical design limits in a cryogenic environment are summarized in Table 8.

Breakdown Due to Helium Leaks

High voltages can be maintained over short distances in a good vacuum. Typically, in the cryostat surrounding CICC and potted magnets, or the vacuum tank surrounding pool-boiling magnets, a vacuum of 10^{-6} to 10^{-5} torr can be maintained. In vacuum systems, where residual gas density is low, the breakdown voltage is to the left of the Paschen minimum. Therefore, electrical integrity within the cryostat can be compromised by helium leaks into the vacuum space. Helium leaks can be caused by diffusion through welds in a conduit, helium feed stubs, and feedthrough seals. If there is a gas leak, the gas density increases and the breakdown voltage is lowered toward the minimum, which could lead to a spark discharge. This is the usual situation in cryostats and junction boxes, where leaks from helium coolant lines or extraction of sensor wires are difficult to suppress completely. Irmisch has confirmed low voltage breakdown in helium gas at cryogenic temperatures and low pressures (58), simulating the effect of a helium leak into a vacuum space with a 10 mm gap. At 6 K, the Paschen minimum was 240 V, instead of the classic minimum of 160 V.

Leaks are suppressed by the avoidance of nonwelded seals, design layouts that permit field repair of leaks, and vigilant leak detection at room temperature and at cryogenic temperatures. Some rules of thumb for leak rate testing are that the leak rate at 1 atmosphere and room temperature is approximately 1000 times better than the leak rate at 10 atmospheres and 4 K. A state-of-the-art measurement, using mass spectrometry, might test helium stubs down to leak rates of 10^{-10} torr-L/s at room temperature, corresponding to $\sim 10^{-7}$ torr-L/s at 4 K.

It is generally acknowledged that quality assurance alone won't guarantee an absence of electrical discharges in vacuum, because of the difficulty of guaranteeing zero leaks and because of the deleterious effects on breakdown of modest transverse magnetic field. Three design ideas have been proposed that can decrease the probability of discharges by several orders of magnitude: (1) grading of the insulating ground planes, (2) the use of a guard vacuum, and (3) the use of insulating beads.

1. The use of graded ground planes around all insulating surfaces has the greatest generality as a design concept. If all metallic surfaces that are facing each other with high potential differences are insulated, then there can't be an arc between those surfaces acting as electrodes; although there could still be partial discharges that would gradually degrade the insulation. However, if each insulating surface or wrap has a ground plane, the resistance of the ground plane can be graded, so that the insulating or ground plane surfaces facing each other never have a potential difference greater than 160 V. In this case, no combination of pulsed fields, capaci-

Table 7. Tracking Strength for 60 kV Pulse Waveforms (kV/cm)

Material	Pressure (atm)	LHe 4 K	GHe 4 K	GHe 293 K	LN2 77 K	GN2 77 K	GN2 293 K
Mylar	0.9	79	<3.6	2.7	158	39	4.7
	1.6	79		2.8	189	79	6.8
Paper phenolic	0.9	95	4.3	2.3	158	32	4.3
	1.6	118	4.3	3.3	189	39	7.9
Polyethylene	0.9	118	3.8	2.6	158	30	5.9
	1.6	158	3.9	2.7	236	59	7.9
Nylon	0.9	79	3.9	2.0	158	47	4.7
	1.6	118	3.9	2.0	236	59	7.9
Teflon	0.9	95		2.8	79	43	4.7
	1.6	158		3.1	158	53	7.9
Permalin	0.9	68		2.2	118	30	4.7
	1.6	79		2.8	158	68	7.9

Table 8. Typical Electrical Insulation Sizing Rules

Type	Units	Design Criterion
Flashover along insulating spacer in helium	V/mil	5–7
	V/mm	100–300
Tracking along insulating wrap	V/mil	1.5–5
	V/mm	60–200
Breakdown through epoxy	V/mil	50–150
	kV/mm	1.5–6
Breakdown through kapton wrap	V/mil	125–500
	kV/mm	5–20

tive charges, or helium pressures can cause a breakdown.

2. The use of a guard vacuum around a winding pack can be very effective, where space constraints aren't significant, as in the Mirror Fusion Test Facility-B (MFTF-B) coils (59). The secondary vacuum space greatly decreases the probability of a leak into the cryostat by requiring two series independent leaks in the coil case and the guard vacuum shell. It can further lessen the possibility of operational problems by the use of independent on-line leak detection and/or differential vacuum pumping. In MFTF-B, it also had a fringe benefit of being used as an auxiliary helium channel to reduce thermal stresses in the winding during cooldown.
3. Fast and Hart (60) have shown that filling an evacuated box for power feedthroughs box with glass beads increased the Paschen minimum voltage and increased the pressure at the Paschen minimum, as shown in Fig. 33. Testing in helium as a function of pressure from 1 Pa to 0.13 MPa (10^{-5} to 1 atm) at room temperature, 77 K, and 4.2 K in helium, they found that the minimum breakdown voltage across a 4.8 mm gap was increased by more than a factor of 10 at all three temperatures. Insulating beads could be used to raise the Paschen minimum by an order of magnitude, either in evacuated spaces, such as junction boxes, or in high pressure chambers, such as helium isolators with filters.

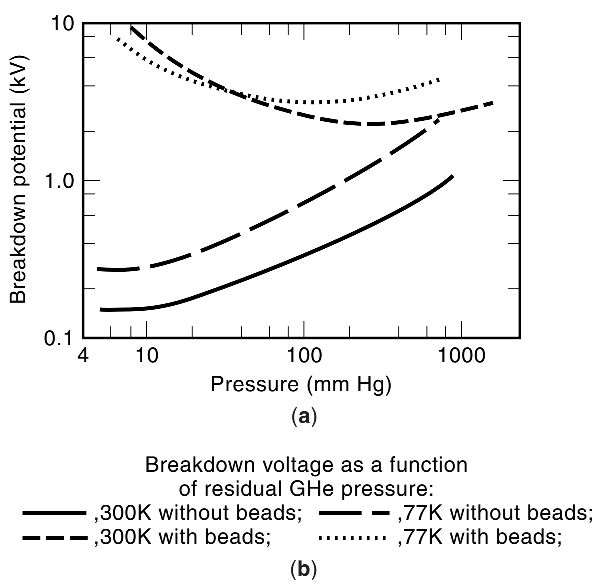

Figure 33. Paschen curve for helium. (a) Measured in uniform gap and (b) measured in gap with and without glass bead particles [Fast and Hart (60)].

CASE HISTORIES

The majority of actual failures to protect superconducting magnets have had little relation to the design principles described in this chapter. Errors in operation have accounted for more failures than errors in fabrication, and errors in design have been less important than either. Several studies and workshops have addressed the problems of real-life magnet protection (61).

Operational errors causing magnet component failures have included:

- Bypassing protective circuits or not replacing them when they fail
- Wiring magnet or instrumentation leads backwards
- Interpreting anomalous or changed sensor readings as indicators of interesting experimental phenomena, instead of burnout
- Poorly written, long and boring operating instruction manuals, with incorrect or ambiguous instructions; the ignoring of instructions
- Absence of routine inspection and replacement of components with finite lifetimes
- Energization of coils in an incorrect sequence (the classic error is energizing an outer solenoid and crushing an inner solenoid with no strength in radial compression through induced diamagnetic currents)
- Increasing current when critical properties proved to be better than expected, leading to burnout of vapor-cooled lead
- Unattended dewar operation leading to ice blocks, causing overpressure in the dewar
- Removal of a rubber stopper in a dewar, leading to inadequate vapor flow to the leads; failure to monitor lead gas flow or voltage drop

Manufacturing QA problems that led to coil or prototype failure included:

- Helium leaks at fittings
- Voids at the conductor/monolith interface leading to mechanical rupture of the conductor
- Small metallic slivers being sprung from a conduit by the tube mill
- Metallic inclusions in an open, pool-boiling magnet causing turn-turn shorts and arcing
- Insulation tearing during winding, especially of kapton
- Joint installation without solder
- Weld contamination due to contamination by injected polyurethane spacers
- Turn-turn short due to mechanical abrasion of insulation during transportation and installation
- Vacuum leaks through mechanical (i.e., nonwelded) seals

- Exposure of Incoloy conduit to oxidants during heat treatment, leading to stress aggravated grain boundary oxidation (SAGBO) cracking

Reliability problems caused by inadequate redundancy in the design of the protection circuits have included:

- Dump circuit interrupters failing to clear
- Power supplies failing to shut down on receiving a correct trigger signal from the protection circuit
- False positive dump signals leading to arcing
- Programming error in a programmable logic controller leading to deliberately applying overcurrent to the coil. Same problem with overvoltage
- Arcing in a dump resistor causing a dump that was too slow

Structural design errors have included:

- An overly complex load path causing structural failure of a brittle, aluminum primary structure
- Inadequate mechanical protection of sensor insulation
- Inadequate mechanical support of leads, causing lead shorting or arcing
- Peeling of solder lap joints from ends, neglecting strain incompatibility

SUMMARY

Superconducting magnet protection during a quench is an important but special case of the larger problem of magnet protection against structural, electrical, and thermal failures. The usual method of guaranteeing protection is to build conservative magnets with more structure, stabilizer, and superconductor than they need. The techniques of providing adequate conservatism in the design of magnet protection circuits, quench detection, protection criteria, quench propagation modeling, and electrical integrity have already been described. However, experience with magnet failures suggests that new design approaches may be more successful in the future.

In most cases, redundancy should be favored, where possible, as a method of guaranteeing reliability, over just adding more material, because of its ability to multiply low probabilities of failure. Redundant techniques include the use of in series, independent interrupters; paralleled independent quench detectors and paralleled independent cowound heaters. It also includes the use of leak-tight welds and guard vacuums, insulation systems with no voids below the Paschen minimum and long discharge or tracking life, and simultaneous use of signal-noise improvement techniques, such as selecting the best spot in the cable for a cowound sensor, differencing, and filtering the optimized signals.

Given the certainty that data processing will continue to improve more rapidly than magnet technology, future magnets are likely to concentrate on using redundancy and intelligent signal processing in order to improve performance and reliability simultaneously. Smart interlocks should check for wiring errors, while simulators check and calibrate sensors. Reviewed projects must adopt more stringent review standards, insisting on a complete design of the protection system, not only of the magnets, but also the leads, bus, and instrumentation feedthroughs. The goals of these improvements would be to achieve orders of magnitude decreases in the probability of failure to detect a quench rapidly, to successfully interrupt current in a magnet, and to simulate and adequately predict the ability of quench propagation to absorb magnet energy without damage.

BIBLIOGRAPHY

1. C. Neumeyer et al., Quench protection circuits for superconducting magnets, *Proc. IEEE Symp. Fusion Energy,* U. Illinois, p. 1275, Sept 30–Oct 5, 1995.
2. P. Dokopoulos and K. Kriechbaum, DC circuit breaker for 73 kA, 24 kV. *Electrotech. Zeitschrift A.* **97** (8): translated by H. Vogel, Los Alamos Report LASL-TR-77-27, 1976.
3. S. Yokota, Poloidal field power supply using vacuum circuit breaker, *IAEA Second Large Tokamak Meeting,* Princeton, New Jersey, Nov. 1976.
4. V. Kuchinski et al., High-power fast switches, *IPEC-Yokohama,* 899, 1995.
5. Argonne National Laboratory Superconducting Magnet Group, Final design of a superconducting MHD magnet for the CFFF, Argonne National Laboratory, ANL-MHD-79-6, pp. 250–251, March, 1979.
6. C. Neumeyer, Liquid rheostat dump resistors, Princeton Plasma Physics Laboratory 40-940217-PPPL/CNeumeyer-01, Feb 17, 1994.
7. T. Ishigohka and Y. Kushiro, Quench protection of superconducting magnet using ZnO arrester, *Cryogenics,* **31**: 562, 1991.
8. A. Dudarev, V. E. Keilin, and Y. Kuroedov, Quench protection of very large superconducting magnets, *IEEE Trans. Appl. Supercond.,* **5**: 226–229, 1995.
9. S. M. Schoenung et al., Liquid helium dump concept for a large scale superconducting magnetic energy storage plant, *Adv. Cryo Eng,* **31**: 1986.
10. J. F. Kaerner et al., A protection system for small high power SMES with power semiconductors working at cryogenic temperatures, *IEEE Trans. on Appl. Supercond.,* **5**: June 1995.
11. O. P. Anashkin et al., Superconducting magnet protection system, *Adv in Cryogenic Eng,* **37**: Part A, 339, Plenum Press, 1992.
12. J. Purcell et al., The superconducting magnet system for the 12-foot Bubble Chamber. Argonne National Laboratory Report ANL/HEP6813, 1968.
13. D. F. Sutter et al., Electrical protection of superconducting magnet systems, Fermi National Laboratory Technical Memorandum TM-559, March 1975.
14. T. Ogitsu et al., Quench observation using quench antennas on RHIC IR quadrupole magnets. *IEEE Trans. Mag.,* **32**: 3098, July 1996.
15. S. J. St. Lorant communication reported in J. Allinger, G. Danby, S. Y. Hsieh, J. Kean, J. Powell and A. Prodell, Fusion magnet safety studies program superconducting magnet protection system and failure: Interim Report. Brookhaven National Laboratory, BNL 20787, Nov 1975.
16. M. Darweschsad, The POLO coil, a prototype tokamak poloidal field coil, design features and test results. MT-14, Tampere, Finland; June 1995.
17. J. H. Schultz, Feasibility of the TPX voltage sensor quench detection system. M.I.T. Plasma Science and Fusion Center Report PSFC/RR-97-3, March 5, 1997.
18. N. Mitchell et al., ITER No: N11 R1 03 04-09-07 W1, Magnet design description: Appendix A: conductor design, April 14, 1995.

19. I. Zatz et al, TPX No: 94-950117-PPPL-IZatz-01, TPX structural and cryogenic design criteria, Rev. 1, Jan 17, 1995.
20. J. H. Schultz, ITER No ITER/US/96/EV-MAG/J.H.SCHULTZ/5.31/-1 J. H. Schultz, P. W. Wang, and S. Smith, Interpretation of voltage sensor data in the QUELL experiment, May 31, 1996.
21. M. M. Steeves et al., The US Demonstration Poloidal Coil. *IEEE Trans. Mag.,* **27**: 2369–2372, 1991.
22. Nicolai N. Martovetsky, and Michael R. Chaplin, Normal-zone detection in tokamak superconducting magnets with co-wound voltage sensors. *IEEE Magnet Technol. Conf.,* Tampere, Finland, July, 1995.
23. P. W. Wang, TPX Memo: 13-930719-MIT-PWANG-01, TF voltage tap noise due to plasma disruption. July 19, 1993.
24. H. T. Yeh, J. S. Goddard, and S. Shen, Inductive voltage compensation in superconducting magnet systems, *8th Symp. Eng. Probs. Fus. Res,* 1802, 1979.
25. S. Smith and S. Ezekiel, TPX No:1314-941130-MIT/SSmith-01, Improved fiberoptic quench detection at the Francis Bitter National Magnet Laboratory. Rev. 1, Nov 30, 1994.
26. J. H. Schultz and S. Smith, TPX Memo 1314-950815-MIT-JSchultz-01, Feasibility of the fiber optic temperature-sensor quench detection system. Aug 15, 1995.
27. S. P. Smith, TPX No:1314-950424-MIT-SSmith-01, Report on fiberoptic strain sensitivity reduction experiments at the Francis Bitter National Magnet Laboratory on 3/16/1995, April 24, 1995.
28. K. Koepke, P. Martin, and M. Kuchnir, Doubler system quench detection threshold. *IEEE Trans. Mag.,* **MAG-19**: 696, May 1983.
29. Y. Iwasa and M. Sinclair, Protection of large superconducting magnets: maximum permissible undetected quench voltage. *Cryogenics,* Dec. 1980.
30. Y. Iwasa, *Case Studies in Superconducting Magnets: Design and Operational Issues.* New York: Plenum Press, 1994.
31. Y. Iwasa, Design and operational issues for 77 K superconducting magnets, *IEEE Trans. Mag.,* **MG-24**: 1211, 1988; Y. Iwasa et al., Stability and quenching in high-temperature superconductors, *IEEE Trans. Appl. Supercond.,* **5**: 389, 1995.
32. C. H. Joshi and Y. Iwasa, Prediction of current decay and terminal voltages in adiabatic superconducting magnets, *Cryogenics,* **29**: 157, 1989.
33. L. R. Turner, Safety of superconducting fusion magnets: twelve problem areas, Argonne National Laboratory Report ANL/FPP/TM-121, May 1979.
34. R. P. Krause and E. H. Christensen, Calculation of quench pressures in pool boiling magnets, *IEEE Trans. Mag.,* 1979.
35. J. Powell, ed., Aspects of safety and reliability for fusion magnet systems. Brookhaven National Laboratory, BNL 50542, 72-75, Jan 1976.
36. J. R. Miller, J. W. Lue, and L. Dresner, *IEEE Trans. Mag.,* **MAG-13** (24): 1977.
37. Z. J. J. Stekly, *Adv. Cryo. Eng.,* **8** (ed.) Timmerhaus K.D. New York, Plenum Press, 1963, 585.
38. L. Bottura and O. C. Zienkiewicz, Quench analysis of large superconducting magnets, *Cryogenics,* **32** (7): 659, 1992; L. Bottura, A numerical model for the analysis of the ITER CICC's, *J. Comp. Phys,* **125** (26): 1996; L. Bottura, Numerical aspects in the simulation of thermohydraulic transients in CICC's. *J. Fusion Eng.,* **14** (1): 13, 1995.
39. L. Dresner, Protection considerations for force-cooled superconductors, *Proc. 11th Symp. Fusion Eng.,* **II**: 1218–1222, Austin TX; Nov. 18–22, 1985.
40. L. Dresner, Thermal expulsion of helium from a quenching cable-in-conduit conductor, *Proc. 9th Symp. Eng. Prob. Fusion Res.,* 618, Chicago, 1981; reformulated in L. Bottura, Quench propagation and protection in cable-in-conduit superconductors. Encyclopedia of Applied Superconductivity, Comett 4090 Cb, 1996.
41. Y. Wachi et al, Investigation of the pressure rise during the quench of a force cooled superconducting coil, *IEEE Trans. Mag.,* **25**: 1500–1503, 1989.
42. A. Shajii and J. P. Freidberg, Quench in superconducting magnets. II. Analytic solution, *J. Appl. Phys.,* **76** (5): 1 Sept 1994; L. Dresner, *IEEE Trans. Mag.,* **25**: 1710, 1989; L. Dresner, *Proc 11th Symp Fus Eng, IEEE,* 1218, **2**: 1986.
43. A. Shajii and J. P. Freidberg, *J. Appl. Phys.,* **76** (5): 1 Sept 1994.
44. A. Shajii, Universal scaling laws for quench and thermal hydraulic quenchback in CICC coils, *IEEE Trans. Appl. Supercond.,* **5**: 477–482, 1995.
45. G. Olivier, Y. Gervais, and D. Mukhedar, A new approach to compute uniform field breakdown of gases, *IEEE Trans. Power Appar. Syst.,* **PAS-97** (3): May/June 1978.
46. Dielectric breakdown of cryogenic gases and liquids. J. Gerhold, *Cryogenics,* Fig. 22, 1979.
47. Meek and Craggs, *Electrical Breakdown of Gases.* 662, Fig. 6.14, New York: Wiley, 1978.
48. J. Gerhold, Dielectric breakdown of cryogenic gases and liquids, Fig. 10, *Cryogenics,* 1979.
49. D. May and H. Krauth, Influence of the electrode surface condition on the breakdown of liquid helium. *IEEE Trans. Mag.,* **MAG-17** (5): Sept 1981.
50. Ch. Olivier, Performance of electrodes at the first voltage breakdown in liquid helium, *IEEE Trans. Mag.,* **MAG-17** (5): Sept. 1981.
51. Fallou, Dielectric breakdown of gaseous He at very low temperatures. *Cryogenics,* April 1970.
52. R. J. Meats, Butt gap discharges in laminated insulation impregnated with very cold helium gas. *Third Int. Conf. Gas Discharges, IEEE,* London, 1974.
53. J. Hiley and R. S. Dhariwal, Dielectric breakdown in high density helium and in helium impregnated solid dielectrics. *Cryogenics,* **25**: 334, June 1985.
54. M. Zahn, Preliminary engineering design criteria to prevent spark discharges in TPX, Nov 27, 1994, TPX Memorandum No. 1314-941127-MIT-MZahn-01.
55. A. M. Miri, Transient voltage oscillations in a large superconductive coil. *9th Int. Symp. High Voltage Eng.,* Graz, Austria, Aug 28–Sept 1, 1994.
56. A. Migliori, R. I. Schermer, and M. D. Henke, Dielectric tracking in liquid helium. *Cryogenics,* 442, 1978.
57. R. A. Haarman and K. D. Williamson, Jr., Electrical breakdown and tracking characteristics of pulsed high voltages in cryogenic helium and nitrogen. *Adv Cryo Eng.* **21** (102): Plenum Press, 1976.
58. M. Irmisch et al, Breakdown characteristic of helium gas at cryogenic temperatures and low pressures with respect to a local helium leak. KFK Report 31-03-05 P02B, June 1992.
59. C. Henning, Reliability of large superconducting magnets through design. *IEEE Trans. Mag.,* **MAG-17** (1): 618, Jan. 1981.
60. R. W. Fast and H. L. Hart, Use of glass beads to increase the breakdown voltage in subatmosphere, cold helium gas. *Advances in Cryogenic Engineering,* **35**: Plenum Press, New York, 1990, 809–812.
61. P. G. Marston et al, Magnet Failure Workshop, Journal de Physique, Colloque C1, Tome 45, Jan 1984, C1-637; F. Arendt and P. Komarek, Potential failures and hazards in superconducting magnet systems for fusion reactors. *Nuc Tech/Fusion,* **1**: Oct, 1981; R. J. Thome, J. Bart Czirr, and J. H. Schultz, Survey of selected magnet failures and accidents.

JOEL H. SCHULTZ
Massachusetts Institute of Technology